RESIN FLOW VELOCITY MEASUREMENT OF CARBON FIBER/EPOXY COMPOSITES IN AUTOCLAVE PROCESSING

A Thesis by

Ashraf Uddin Ahmed

Bachelor of Science, Bangladesh University of Engineering and Technology, 2006

Submitted to the Department of Mechanical Engineering
and the faculty of the Graduate School of
Wichita State University
in partial fulfillment of
the requirements for the degree of
Master of Science

May 2012

RESIN FLOW VELOCITY MEASUREMENT OF CARBON FIBER/EPOXY COMPOSITES IN AUTOCLAVE PROCESSING

The following faculty members have examined the final copy of this thesis for form and content, and recommend that it be accepted in partial fulfillment of the requirement for the degree of Master of Science with a major in Mechanical Engineering.

_____
Bob Minaie, Committee Chair

_____
Hamid Lankarani, Committee Member

_____
Krishna Krishnan, Committee Member

DEDICATION

To my parents, my wife, my brother and my sister

ACKNOWLEDGEMENTS

I would like to thank my advisor, Dr. Bob Minaie, for his valuable advice and guidance to perform this study. I would also like to thank Dr. Hamid Lankarani and Dr. Krishna Krishnan for serving on my thesis committee.

I am grateful to Behrouz Tavakol for his encouragement throughout this study. I would like to express my gratitude to my team members Pooneh Roozbehjavan, Rony Das, Ronald Joven and Mohammad Amdadul Islam for their comments and discussions on the experimental work. Many thanks to Khalil Vora and Tien Vo for their invaluable discussions on resin rheology. I am grateful to Richard Prevost of the LaVision Inc. for his technical support on Davis software. Special thanks to Chee Sern Lim for his helpful technical comments and thoughts. I would like to thank Saw Kee Hong, Mohammad Habibi, Mauricio Guzman, Hoda Koushyar, Nita Yodo, Dr. Seyed Soltani, Dr. Alejandro Rodriguez, Joey Schaefer and Shannon Walker for their friendship and support during my stay at the laboratory.

Financial support by the National Aeronautics and Space Administration (NASA) is gratefully acknowledged.

ABSTRACT

The resin flow during composite processing affects the mechanical properties and the final dimensions of the part. This study investigates resin flow velocity in autoclave processing. To measure the resin flow velocity during cure, a flow apparatus was designed and manufactured with the ability to follow the autoclave curing cycle. Resin flow tests were conducted on IM7/977-2 unidirectional laminates seeded with fluorescent polymer particles which were tracked during cure. Particle image velocimetry and particle tracking velocimetry techniques were applied individually to obtain resin flow velocity and flow pattern during cure. In addition to the peak resin velocity, corresponding time of peak velocity and flow cessation times were investigated during the test. Moreover, the effect of curing parameters such as heating rate, pressure, vacuum, and isothermal temperature on the resin flow were also studied.

For unidirectional laminate peak resin velocity in longitudinal direction was an order of magnitude higher than the peak velocity in the transverse direction. Experimental results showed that the peak velocity in longitudinal direction was very close to the maximum velocity of the resin flow test. It was observed that resin reached its peak velocity before attaining its minimum viscosity, then slowed significantly before reaching the gel point.

Finally, the resin flow study was further extended for plain weave material. Resin flow was observed in between the tow borders as well as in the tows of the specimen. In regards to plain weave material, resin peak velocities in both longitudinal and transverse directions were of the same order of magnitude.

TABLE OF CONTENTS

TABLE OF CONTENTS (continued)

LIST OF TABLES

LIST OF FIGURES

LIST OF FIGURES (continued)

LIST OF FIGURES (continued)

LIST OF FIGURES (continued)

LIST OF ABBREVIATIONS

ASTM	American Society for Testing and Material
CCD	Charged Coupled Device
CTE	Coefficient of Thermal Expansion
FOV	Field Of View
IR	Interrogation Region
LDV	Laser Doppler Velocimetry
PIV	Particle Image Velocimetry
PTU	Programmable Timing Unit
PTV	Particle Tracking Velocimetry
PW	Plain Weave
RFI	Resin Film Infusion
SEM	Scanning Electron Microscope
UD	Unidirectional
VBO	Vacuum Bagging Only
WDX	Wavelength Dispersive X-ray

LIST OF SYMBOLS

α	Degree of cure
η^*	Complex viscosity
η'	Resin dynamic viscosity
η''	Elastic part of complex viscosity
G^*	Complex shear modulus
T	Temperature
V_f	Fiber volume fraction
$\overline{\sigma}$	Effective stress (load carried by fibers)
k	Permeability
k_x	Permeability in fiber direction
k_z	Permeability in through thickness
r_f	Fiber radius
K	Kozeny constant
K_1	Kozeny constant in fiber direction
K_2	Kozeny constant in transverse direction
R_e	Reynolds number
μ	Viscosity
L	Length
σ	Applied load on laminate
P	Load carried by resin
m_v	Coefficient of volume change

u_∞	Settling velocity
d_p	Particle diameter
ρ_p	Particle material density
ρ_f	Fluid density
g	Gravitational acceleration
V_x	Velocity component in longitudinal direction
V_y	Velocity component in transverse direction
V_{xmax}	Maximum longitudinal velocity over specimen or section
V_{ymax}	Maximum transverse velocity over specimen or section
V_{xpeak}	Peak longitudinal velocity of the test (Peak velocity of UD)
V_{ypeak}	Peak transverse velocity of the test

CHAPTER 1

INTRODUCTION

1.1 Motivation and Scope

Manufacturing costs are always a great concern when attempting to create high quality composite parts. Among the various composite manufacturing processes, hand layup is used in low cost and small scale production while, resin transfer moulding, compression moulding, filament winding and pultrusion winding manufacturing methods are widely used in large scale production. For high performance application parts such as aerospace application, autoclave processing is very commonly used. Generally in autoclave processing, prepregs made with fibers pre-impregnated with partially cured thermoset resin are cured at high temperatures. The curing process as a whole determines the quality of the resulting composite part which has to meet certain criteria. The curing process includes heating and cooling rate, appropriate cure temperature, vacuum and pressure, curing stage, dwell time, pressure window time. A good quality cured composite part has the required fiber volume fraction, minimal void content, dimensional accuracy, and low distortion. To obtain such parts, parameters of composite curing must be optimized. Previously, this optimization was reached using trial and error experimental results, but now, computational processes are being implemented to achieve a cost effective and faster optimization.

In general, the fiber volume fraction of a laminate determines its mechanical and thermal properties. Initially when prepregs are fabricated, they contain excess resin that bleeds off during the curing process, giving the laminate the required fiber volume fraction. Excess or low bleeding of resin during cure leaves a laminate lacking or too rich in resin, altering the required properties. A resin rich area causes properties such as low strength and high co-efficient of

thermal expansion (CTE) while a lack of resin causes fiber contacts and improper load distribution. Moreover, voids, another issue in improperly cured composites, are generated in the laminate for many reasons. For example, they may be caused by trapped air bubbles during resin mixing, carried with particles within the curing agent, or created from broken fibers and air pockets developed during layup. These voids migrate or diminish with resin flow in the laminate.

Distortion induced from residual stresses during the curing process is one of the major causes of loss of dimensional accuracy in final composite parts. Development of residual stress during cure can be attributed to several factors such as material anisotropy, tool part interaction, and cure shrinkage during processing. Anisotropy or directional dependency is an inherent property of composite material. Properties like CTE in a composite part are higher in the resin dominated direction than in the fiber dominated direction. Uncured composite prepregs are laid up and cured on tools of aluminum, steel, and Inver to achieve a desired shape. Mismatch of CTE in tools and composite parts causes different expansion and residual stresses to develop due to friction exerted over the part by the tool. Cure shrinkage is the total effect of consolidation, chemical shrinkage, and resin flow. Laminates decrease in thickness due to consolidation, leaving thinner plies on top and thicker plies on the bottom. The resin polymerization causes shrinkage in its volume. Finally, excess resin flowing out of the laminate during cure causes shrinkage in the laminate thickness.

During processing of laminated composites, resin flow is one of the most critical issues affecting fiber volume fraction, void content, and dimensional accuracy of the final part. Still, industries have to confront with uncontrolled resin flow while processing composite parts, especially in autoclave processing where prepregs are used. In industries where dry fiber preforms are used, resin flow can be determined by measuring wave front using a transparent

mold. However, for autoclave processing of prepregs no methods are available to obtain resin flow velocity directly during cure. Generally, resin flow in the laminate is measured on the basis of loss of resin mass from the laminate. Among various available methods, the increase of mass in the bleeder, level of consolidation, and change in laminate thicknesses are most commonly used for measuring resin flow. Although these methods provide bulk flow rate with time, information about velocity pattern or velocity profile are not available from these tests. The ability to measure resin velocity in three directions inside a laminated composite, especially in or near the critical points like bends in complex shapes of the laminate would be useful in solving flow related issues.

Generally, flow measurement techniques include pitot static tubes, hot wire anemometry, laser doppler velocimetry (LDV) and flow visualization techniques like particle image velocimetry (PIV) and particle tracking velocimetry (PTV). Pitot static, hot wire anemometry, and LDV are accurate techniques capable of measuring velocity components in different directions, but they are limited to a single point measurement. Moreover, pitot static and hotwire anemometry require insertion of a probe that can impede flow velocity when the cross section of the flow area is small. Flow visualization techniques, such as PIV and PTV are capable of providing instantaneous velocity components in multiple directions with high accuracy. The basic difference between PIV and PTV is that PIV works on a pattern of particles whereas PTV works on a single particle.

PIV and PTV techniques can be applied on the curing laminate to obtain resin flow information. The present work is an approach to apply simplest 2D PIV and PTV techniques on laminate to extract during cure velocity information of the prepreg laminate. Therefore, a resin

flow apparatus was designed and manufactured and used to investigate resin velocity, velocity profile, flow path and the effect of different parameters of curing on resin flow.

1.2 Thesis Overview

This study is focused on developing an apparatus to apply PIV and PTV techniques to laminate curing to measure the resin flow velocity and investigate the effect of different parameters on resin flow. Materials used for this investigation include IM7/977-2 unidirectional (UD) and plain weave (PW) carbon fiber reinforced epoxies. The specific objectives of this research include:

- Design and manufacture resin flow apparatus
- Investigate appropriate particle and particle distribution for resin flow test
- Measure resin velocity on laminate surface and specimen mid-section
- Measure time and temperature of the peak velocity and flow cessation of the laminate
- Obtain flow pattern or flow path
- Observe the effect of temperature ramp rate and isothermal temperature on resin flow
- Observe the effect of applied pressure on resin flow
- Observe the effect of vacuum pressure on resin flow
- Observe resin flow in plain weave laminate

In this thesis, the objectives are covered in the following sequence: Chapter 2, Literature Review, provides a comprehensive discussion of previous work on resin flow and PIV and PTV techniques to elucidate the objective of this work. In Chapter 3, Technical Approach, design concept of the experimental setup such as flow apparatus, analysis parameters, specimen preparation, and test conditions are explained in detail. Chapter 4, Results and Discussions, includes results from different tests and comparison with previous studies available in literature.

Finally, in Chapter 5, conclusions of this thesis are drawn and possible future works are suggested.

CHAPTER 2

LITERATURE REVIEW

2.1 Theoretical Background

The resin flow in a laminate is one of the major contributors to void formation, transportation, and growth [1, 2]. During processing, because of pressure application and decreased viscosity of resin, excess resin between fibers in tows and adjacent plies move, causing voids to swipe out of the laminate [3]. Several consequences such as thickness variation, residual stresses, and subsequent distortion in the final geometry of composite parts are caused due to resin flow in laminate during cure. To estimate such effects, it is crucial to know resin flow during cure in different directions. Cure shrinkage models for laminated composite consists of several sub models such as the coefficient of thermal expansion, chemical shrinkage, and flow of resin [4]. If any of these factors are not considered, distortion of the final part and its final thickness cannot be accurately estimated.

The curing process is the formation of molecular crosslinks in the resin [5]. The extent of the polymerization reaction is represented by the degree of cure (α). Resin in prepregs is cured to B-stage where linear molecular chains are connected by Van-der Waals bonds. Initially, resin curing is dominated by a viscous effect but as the cross-linking proceeds among linear molecules, an infinite network called gel point starts forming where resin behaves like a viscoelastic material. Eventually, a fully cured solid polymer with increased stiffness and density of network due to continued cross-linking reactions is obtained. Because resin behaves like a viscoelastic material during cure, resin viscosity is represented by complex viscosity (η^*) which is the combination of resin dynamic viscosity (η') and the out of phase or elastic part of the complex viscosity (η'').

$$\eta^* = \eta' - i\eta'' \quad (1)$$

η' and η'' are determined respectively from the loss and storage part of the complex shear modulus (G*).

The resin flow mainly occurs due to applied pressure gradients and viscosity changes. The resin flow rate is controlled by the resin and surrounding pressure of the laminate, resin viscosity, specific permeability, porosity of the fiber bed and laminate dimensions [6]. Resin flow in laminate is quasi-static and transient in nature [6, 7]. The initial viscosity of resin in liquid stage is influenced by size of molecular extension (α) and temperature (T). As resin approaches gel point, viscosity rises rapidly and resin flow ceases.

Fiber beds in laminated composites are considered as a porous elastic medium made of incompressible fibers and saturated with incompressible resin. During processing, resin flows between fibers, keeping fiber mass constant. For ideal packing of fibers with a square and hexagonal array, shown in Figure 1, maximum fiber volume fractions are 78.5% and 90.4% respectively. With this packing, if the fibers are straight, the fiber bed can be represented as a solid with diamond and triangular pores as shown in Figure 1. Under real conditions, the fiber bed pore shape may not be constant and fibers have slight waviness with a length to height ratio of 150 [8]. Gutoswki et al.[9] observed poor fiber alignment when fiber volume fraction (V_f) < 0.785.

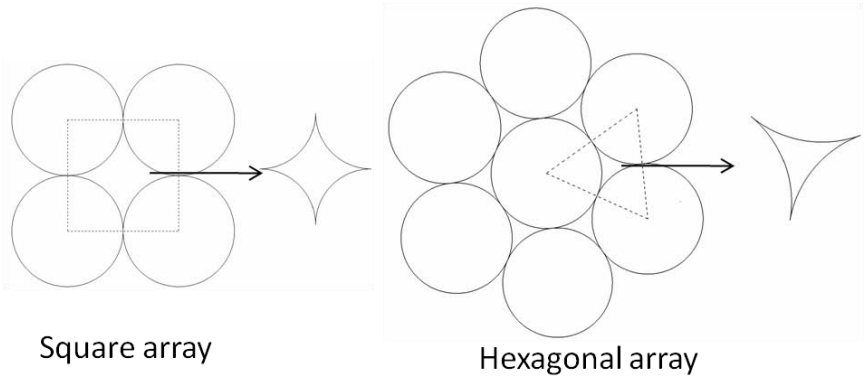

Figure 1. Porous structure for different fiber arrangement.

During cure, the applied pressure on the composite is carried by fiber and resin [6, 10]. Dave et al. [6] concluded that the resin pressure gradient is nonlinear. Over time, resin loses its pressure, transferring the load over the porous fiber bed. Simultaneously, due to the transferred load, compaction in the fiber bed starts. The load carried by the fiber bed structure is called effective stress ($\bar{\sigma}$). The mechanical analogy of the compaction/consolidation process is best described by Taylor [11]. The fiber bed saturated with resin can be compared to a spring immersed in a water tight cylinder with a stopcock (valve) which is filled with incompressible liquid. The stopcock opening represents the permeability of the fiber bed. Compaction time varies with compressibility and permeability of the fiber bed. Gutowski et al. [8] conducted consolidation experiments on carbon fibers impregnated with low viscous oil and found that at $V_f > 0.5$ fibers gradually take an increasing portion of load. He explained the behavior was due to multiple fiber to fiber contacts. Gutowski [12] evaluated the nonlinear relationship between void ratio (e) and effective stress carried by the fiber bed. Dave et al. [10] divided the void ratio (e) - effective stress ($\bar{\sigma}$) relationship into three segments: linear, primary and secondary compression as shown in Figure 2.

At $0< \bar{\sigma} <0.07$ MPa (10 psi), the relation between e and $\bar{\sigma}$ is linear and immediate response occurs after load application. For $0.07< \bar{\sigma} <1.03$ MPa (150 psi), primary compression of

the fiber bed occurs. The relationship curve becomes semi-logarithmic and the fiber bed behaves like a rapidly stiffening spring. Dave et al. [6] observed a rapid pressure drop of resin at this stage. At $\overline{\sigma}$ >1.03 MPa, secondary compression or over consolidation starts.

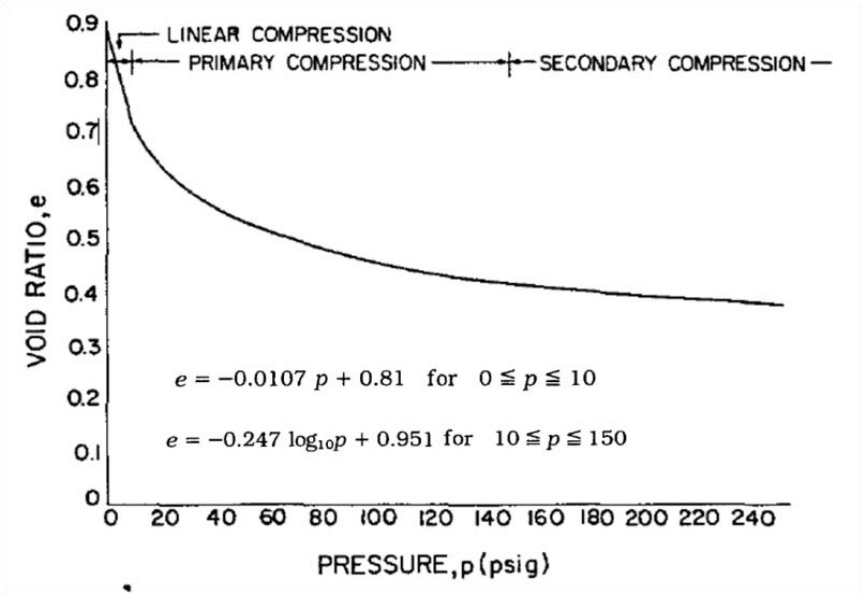

Figure 2. Void ratio and effective stress (p=$\overline{\sigma}$) relationship for stacked graphite fibers [10].

The fiber bed permeability (k) is analogues to the conductivity of the porous media. The more permeable the fiber bed, the less resistance resin faces to flow. According to soil science, permeability is the specific discharge per unit hydraulic gradient [13]. Permeability of the fiber bed may change with time due to an applied external load that changes the structures and texture of the porous bed. As the fiber volume fraction changes during compaction, therefore, fiber bed permeability is a function of fiber volume fraction. Dave et al.[6, 10] described the permeability of laminate fiber bed using Carman-Kozeny equation (1).

$$k = \frac{r_f}{4K} \frac{(1 - V_f)^3}{V_f^2} \tag{2}$$

Where r_f and K are the fiber radius and Kozeny constant, respectively. Anisotropy of the fiber bed permeability is determined by the Kozeny constant in three principle directions. The

principle directions of the laminate are shown in Figure 3. Since fiber bed is assumed to be transversely isotropic, permeability in fiber (1,x) and transverse (2,y) directions are different. Gutowski et al. [8] found axial and transverse Kozeny constant to be K_1=0.7 and K_2=17.9 for different fiber volume fractions. Lam and Kardos [14] reported a Kozeny constant for transverse permeability of K_2=11 for $0.5<V_f<0.75$ and observed substantial decrease in K_2 at higher fiber volume fractions from their permeability experiment. They obtained axial permeability K_1=0.35 and 0.68 for silicone oil and water respectively, indicating the effect of fluid properties on fiber bed permeability. Since laminate contains layers of varying permeability, layers having the highest permeability govern the resin flow [7]. Combining the void ratio and effective stress relationship with Equation 2 provides a relationship of permeability with the effective stress. Figure 4 shows that fiber bed permeability decreases with the increase in effective load.

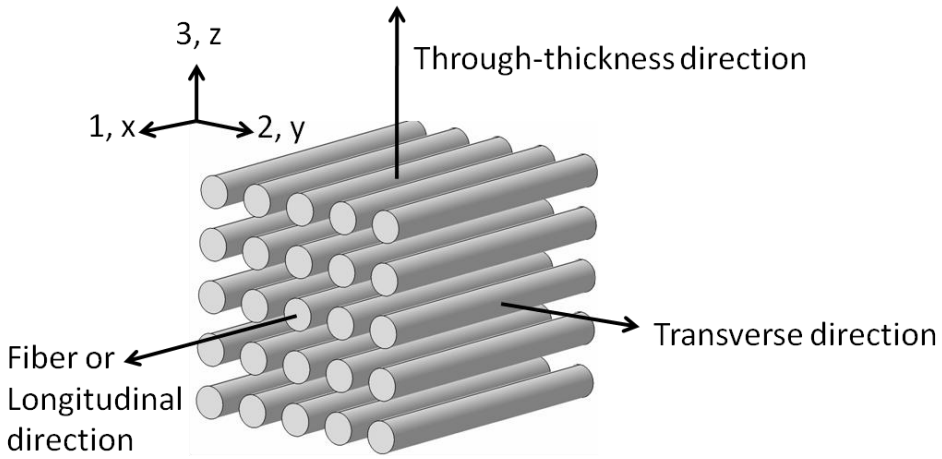

Figure 3. Unidirectional fiber bundle with direction convention.

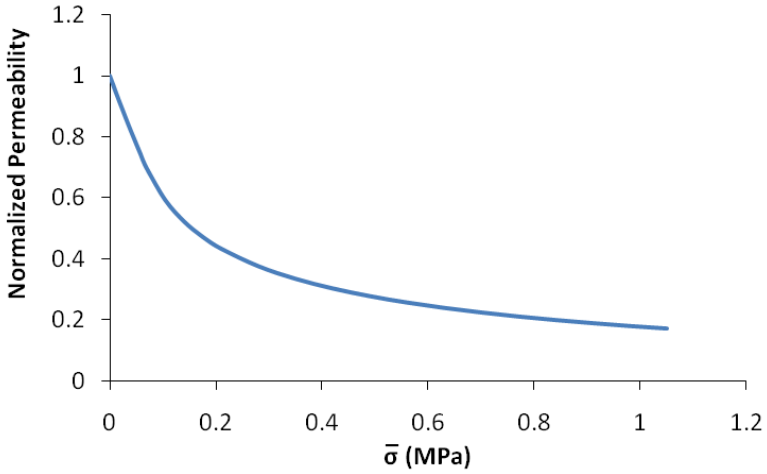

Figure 4. Permeability and effective stress relationship.

Two major mathematical models for resin flow in laminate during cure have been found in literature. The first one is based on the theories of soil mechanics, considering the fiber bed of the laminate as a porous solid. The other follows lubrication theory. Available experimental results support the first modeling approach to a greater degree.

Models based on soil science assumes a pressure gradient across the vertical and horizontal direction of the laminate. While Loos and Springer [15] assumed a linear pressure gradient, Dave et al. [6] and Gutowski [16] considered nonlinear pressure gradients. Resin flow in a laminated composite is laminar and low Reynolds number flow [6]. The porous medium combined with a low Reynolds number (Re≤10) flow can be characterized by Darcy's Law [13]. As a porous medium, flow inside the laminate is described by Darcy's law and requires the knowledge of fiber network permeability, viscosity, and pressure gradient of the resin during cure. According to Darcy's law, resin velocity (V) inside laminate is,

$$V = \frac{k}{\mu}\frac{\Delta P}{L} \tag{3}$$

where μ, ΔP are the viscosity and pressure gradient of the resin and k, L are the fiber bed permeability and length of fiber bed, respectively. Although Darcy's law is suitable for one

dimensional flow, this equation can be applied to three dimensional flow as well [6]. Loos and Springer [15] and Dave et al. [6, 10] use Darcy's law to model resin flow in laminates during cure.

Loos and Springer combined Darcy's law with sequential consolidation in their resin flow model. In sequential consolidation, with the application of pressure, the top ply is pushed towards the second ply, squeezing the resin out between these two plies. As the top ply approaches the second ply, they move together towards the third ply, squeezing resin out throughout the compacted region. When resin moves during consolidation, fiber layers do not resist compaction nor do they take any load applied to the laminate. These assumptions imply that there is a pressure drop across the region that are consolidating while the rest of the plies are under applied pressure. The Loos-Springer model decoupled the resin flow in the directions parallel and normal to the tool plate. Darcy's law was used to model resin flow normal to tool plate. Flow parallel to tool plate was modeled as viscous channel flow between two parallel plates. Center pressure of the laminate is considered to be same and calculated by the balance of applied force. Using the conservation of mass, total resin flow is calculated by the summation of resin flow in parallel and perpendicular directions.

Dave et al. combined Darcy's law with the spring behavior of fiber bed during compaction. Their model is based on the results of the consolidation experiments of Gutowski [12]. During compaction, as contacts between fibers increases, fibers take more loads as they are applied to the laminate. At any point in the laminate, stress can be found from the following equation

$$\sigma = \overline{\sigma} + P \tag{4}$$

where σ and P are applied stress and resin pressure, respectively. This model considers one resin pressure throughout the entire laminate at a particular instant until the laminate is fully compacted and resin pressure drops to zero. Dave et al. derived a differential equation that satisfies the consolidation of a porous bed with three dimensional flow due to one dimensional compression within a given time interval. They assumed

i. A constant boundary condition during compaction process
ii. The permeability was independent of position along a direction
iii. The laminate was unidirectional
iv. The composite laminate had a larger length and width compared to thickness
v. A smaller permeability (i.e larger Kozeny constant) in the direction perpendicular to the fiber.

Their governing differential equation follows.

$$\frac{1}{\mu m_v}\left[k_x\left(\frac{\partial^2 P}{\partial x^2}\right)+k_z\left(\frac{\partial^2 P}{\partial z^2}\right)\right]=\frac{\partial P}{\partial t} \tag{5}$$

where m_v is the coefficient of volume change defined as the ratio of axial strain to axial stress for vertical compression on constrained body, k_x and k_y are permeabilities in *x* and *z* direction, and t is the time. Assumption iv and v automatically neglects the flow in transverse direction.

While a complete theoretical model is presented in [6], results of the proposed model are given in Dave et al. [10]. They obtain nonlinear resin pressure profiles in both fiber and through thickness directions on horizontal and vertical mid-planes of 64,128, and 256 ply laminate with time as shown in Figure 5. As can be seen, both resin pressure and pressure gradient along the mid-plane are higher at 10 minutes in all laminates. With time, both resin pressure and pressure gradient decrease. The velocity profiles on the same planes for 64, 128, and 256 plies for fiber and through thickness direction are shown in Figure 6. Dave et al used the Springer viscosity

relation to characterize Hercules 3501-6 resin for their simulation. Maximum velocity for 64,128, and 256 plies are reported to be 3 µm/s, 5 µm/s and 8 µm/s respectively in fiber direction and 2 µm/s in through thickness direction for all laminates. Moreover, maximum velocity in through-thickness direction for all laminates and in fiber direction for 128 and 256 plies was reported at 20th minute. For the 64 plies, maximum velocity in fiber direction occurred at 10th minute. This model showed that resin flow ceased completely after 40 minutes as the resin pressure profile drops to zero by that time.

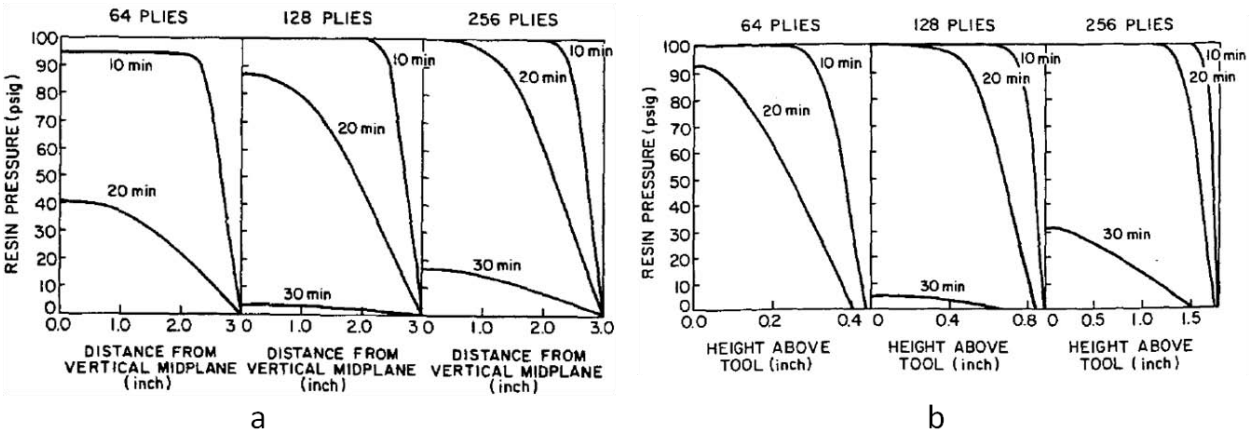

Figure 5. Resin pressure profiles of 64, 128 and 256 ply laminate in a) horizontal mid-planes b) vertical mid-planes [10].

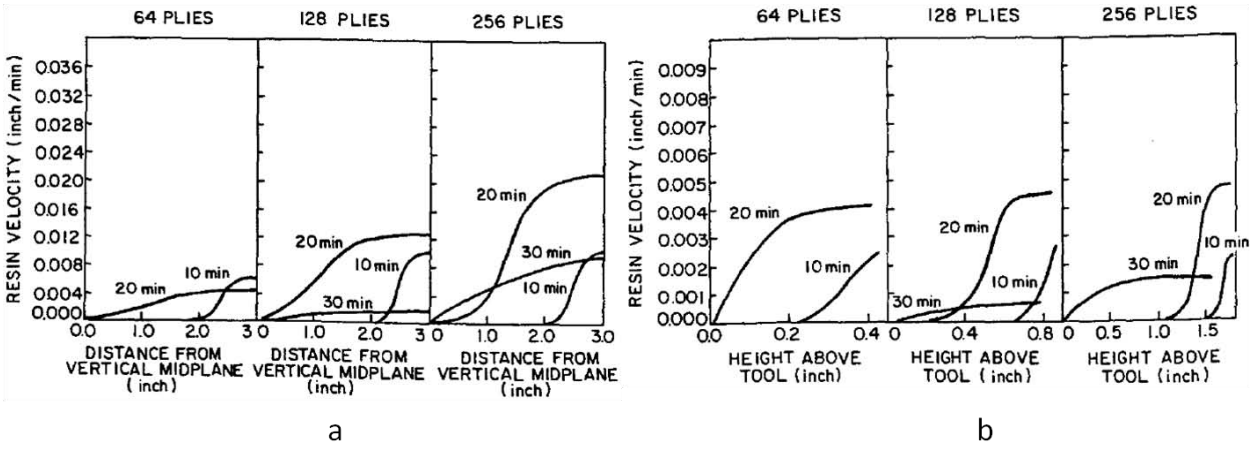

Figure 6. Resin velocity profiles of 64, 128 and 256 ply laminate in a) horizontal mid-planes b) vertical mid-planes [10].

The main difference between the Loos-Springer and Dave et al. models are that the former considers resin flow through porous medium without sharing any load with said medium. Smith and Poursartip [17] studied both models extensively and concluded that the Loos-Springer model is a special case for the Dave et al. model and the latter one describes the compaction process more accurately. They found that fiber bed stress-strain relations influence the resin pressure distribution and laminate compaction behavior to a greater extent.

Lindt [18] used lubrication theory to model flow components created by the compaction of laminates. Fibers are assumed to be rigid and parallel, arranged in square arrays. Resin moves due to drag flow and the squeezing effect between stiff fibers approaching each other. According to their assumptions, fibers do not contact each other and do not carry any load during compaction.

2.2 Experimental Background

Because of the nature of laminated composites, determining resin flow behavior while curing in an autoclave is difficult. Small scale fibers (5 μm diameter [19]) and resin, non-uniform placement of fibers in tow, deformability of fibers and fiber bed, and numerous processing factors like temperature, heating rate, and pressure gradient all affects the flow. Furthermore, resin flow study in autoclave processing becomes more complicated due to flow parallel and perpendicular to the tool plate. In other composite manufacturing processes such as resin transfer molding where dry fiber perform is used, resin velocity can be measured by flow front during processing.

Many researchers [3, 7, 15] previously determined resin flow by loss of laminate mass parallel and perpendicular to the tool plate. In these experiments, laminates were confined in one direction and resin was allowed to flow in the other while a load was applied in the through-

thickness direction. The loss of mass in the laminate could be obtained by measuring the mass of the bleeder before and after cure cycle. To determine resin flow with time, curing is terminated at a specified time within cure cycle and resin flow is measured. Hubert [7] extended his study for flow and compaction behavior of nonlinear shapes of the laminated composites. A detailed explanation of resin flow measurement method by mass is available in ASTM D3531 [20]. Although the loss of mass method is used to verify model results, this method is limited to some extent. The resin flow path and the source of the extracted resin cannot be obtained using this method.

Poursartip et al. [21], used bromine tags in their experimental study to measure resin flow and mixing during cure. They omit the possibility of diffusion of tagging material and determined the flow from WDX (Wavelength Dispersive X-ray) analysis of the specimen using a scanning electron microscope (SEM). They used a measurement volume of 90×70×5 μm to represent a layer when measurements were taken on surfaces parallel to fibers, since the depth of the measurement volume was larger than fiber radius. Plies of tagged prepreg were laid up with untagged prepregs. The laminate was then cured and sectioned for analysis. Since the position of the tagged ply was known prior to cure, the position of the bromine atom was traced after cure by creating a contour map of brominated resin. The distribution of bromine demonstrates the path and amount of resin flow. Although this technique illustrates both qualitative and quantitative resin flow within a laminate for bleed and no-bleed systems, it is very time consuming and provides only the final results. This method cannot provide the flow progress with time.

Thomas et al. [22] used ultrasound C-scan reflectivity to measure the through-thickness resin flow and permeability of a single layer of out-of-autoclave vacuum bag only (VBO)

material at a low and constant temperature (70°C). They used the resin film infusion (RFI) technique to prepare specimens from plain weave carbon fabric. Resin flow rate and permeability of fiber tows were calculated from the measured reflectivity data and Darcy's law respectively. Average resin flow rate were reported as 1.1μm/s in parallel and 0.6μm/s in perpendicular directions to the tool plate. They observed largest the change in reflectivity (i.e maximum velocity) in the space between tows. Although this method provides a good qualitative and quantitative resin flow in laminate without the destruction of the specimen, it is limited by the maximum service temperature of the transducer since autoclave materials are processed at much higher temperatures (180°C). Moreover, processing parameters such as temperature ramp affects C-scan images which can cause extensive errors.

Wartewig et al. [23] measured the degree of cure and gelation of an epoxy resin by investigating the rotation of fluorescent probes in the resin. Since viscosity increases at gel point, it can be found by looking for a reduction in the rotational mobility of the probe molecule. Translational movements of this type of fluorescent probe can be used to obtain the resin flow rate accurately.

Mackenzie [24] developed a tube sensor to measure the hydrostatic resin pressure in the laminate. According to his observation, resin pressure in the laminate increases with pressure application until resin starts flowing. As resin flow starts, pressure drops more and more through the laminate thickness from the top surface to tool surface of the laminate. Furthermore, he observed a pressure gradient across the laminate's thickness until complete compaction of the laminate occurred. From this he concluded that initial degree of cure substantially affects the resin flow and compaction behavior of the laminate.

Alavi-Soltani [25] extensively studied the rheological properties of 977-2 unidirectional (UD) composite material using an ATD CSS 2000 rheometer. Figure 7 shows the complex viscosity, degree of cure, and cure temperature of 977-2 UD material while cured at 177 °C for 180 minutes. Samples are cured from a beginning temperature of 23 °C with a heating rate of 2.8 °C/min. In his experiments, he varied the dwell temperature during cure with the same heating rate and measured a time range of 34-40 minutes for minimum viscosity. Figure 8 shows the minimum viscosity time of 977-2 UD obtained by Alavi-Soltani. The measured average minimum viscosity time for this material is 36 minutes while the gel time for this material was 77 minutes.

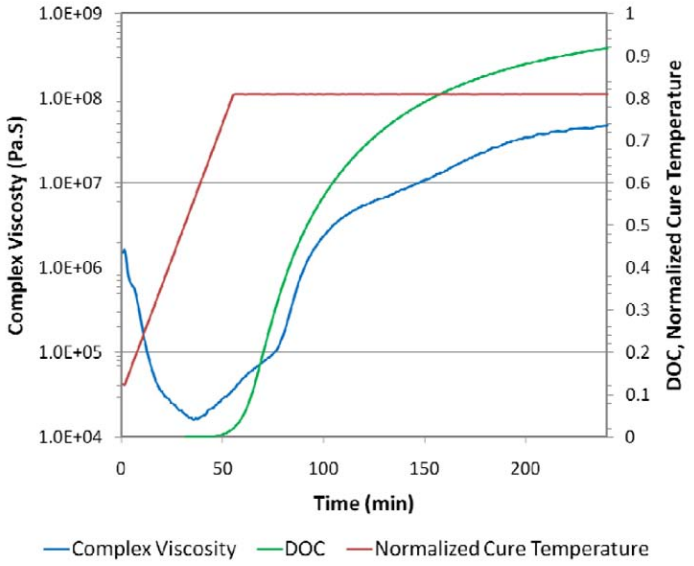

Figure 7. During cure complex viscosity, degree of cure and cure temperature profiles for IM7/977-2 UD [25].

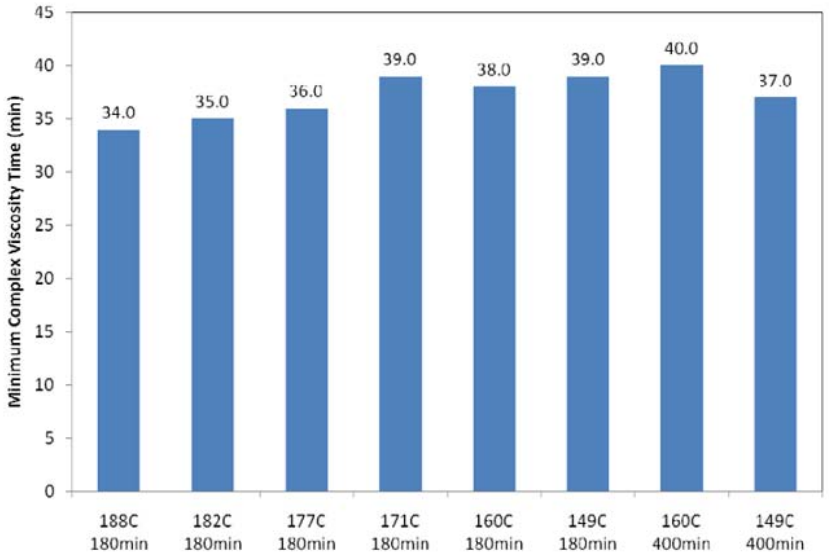

Figure 8. Minimum viscosity times of IM7/977-2 UD at heating rate of 2.8 °C/min [25].

2.3 Flow Measurement Technique

Particle image velocimetry (PIV) and Particle tracking velocimetry (PTV) are two powerful techniques to visualize flow and measure the velocity of moving fluids [26]. While PIV works on image patterns created by using particles, PTV works on individual particles [26-28]. Single-frame, single-exposure image cross correlation was used in this study and a detailed theoretical background is available in [29-31]. Particles used for flow measurements should have similar density of the flowing fluid to minimize error induced due to gravity [30]. Particles/tracer patterns are assumed to exactly follow the fluid motion, not to have any impact on the fluid flow or its properties and does not interact with each other [31]. The main criterion for selecting a particle was its settling velocity (u_∞) in the flow. Expression for u_∞ is

$$u_\infty = \frac{g d_p^2 (\rho_p - \rho_f)}{18\mu} \tag{6}$$

where μ and ρ_f are viscosity and density of the fluid, respectively; d_p and ρ_p are particle diameter and density, respectively; and g is the gravitational acceleration. Particles with negligible u_∞ compared to the flow velocity were chosen. Choosing particles with small

diameters and densities close to the density of the flowing medium kept the u_∞ negligible compared to the flow.

A complete PIV/ PTV system requires four basic components [26, 30, 32]: a transparent system that contains flow seeded with tracer particles, a light source to illuminate the particles, and a camera (CCD(charged coupled device) or film) to record the particle movement. Light sources can vary from a normal bulb to an expensive laser depending on the particles and measurement system. Depending on the number of cameras, velocity components of the flow can be measured. A minimum of two cameras are required to measure 3D flow [30]. For convenience, CCD cameras are used more than film cameras in PIV/PTV measurements. Finally, to process the recorded images and extract velocity information, a computer with a suitable software or algorithm is required. A schematic of the system is shown in Figure 9 .

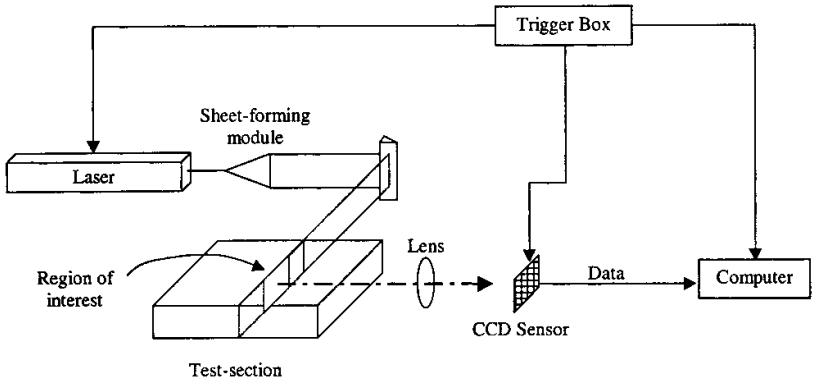

Figure 9. Basic components of PIV system [26].

The algorithms used for extracting displacement or velocity information are either auto-correlation or cross correlation. While auto-correlation is applied on single frame double exposure image, cross-correlation is applied on single frame, single exposure images. In our study of resin flow in laminated composites, cross-correlation of single frame, single exposure images were used for analyzing consecutive frames taken by a CCD camera. A simple example of the cross-correlation of double frame single exposure images, are given below in Figure 10.

As pixels are the construction unit of digital images, the whole image is divided into interrogation regions (IR) containing pixels. Figure 10 (i) represents two consecutive frames of 7×7 pixels taken at a time difference Δt where the particle image pattern of 3×3 pixels in frame A moved to a position in frame B. The IR that consists of 3×3 pixels is shown with the pattern and red boundary from frame A. Each pixel that contains nonzero intensity is marked with blue color and has a value of 1 while zero intensity pixels are valued at 0. This interrogation region from A, was searched over frame B to get the exact match of the pattern. Pattern matching is represented by cross correlation value and the pixel matching is marked with green pixels in the figure. Cross correlation values were calculated by summing the multiplication of overlapping pixel values. Initially, for IR pattern displacement (0,0), the correlation value was 1, due to only one pixel matching in the IR pattern with frame B. For IR displacement of (1,0), (2,0) and (2,1), the correlation value became 0, 2, and 0 respectively as shown in Figure 10 (iii-v). The peak correlation value was 5, which shows the best match obtained for the displacement (2,2) as shown in Figure 10 (vi). A cross correlation map presenting correlation values on the separation plane is shown in Figure 10 (vii) from the point at which the displacement vector of the IR is obtained. For this example the obtained vector is $2\underline{i}+2\underline{j}$. A full theoretical description of the cross correlation technique is available in [29-31].

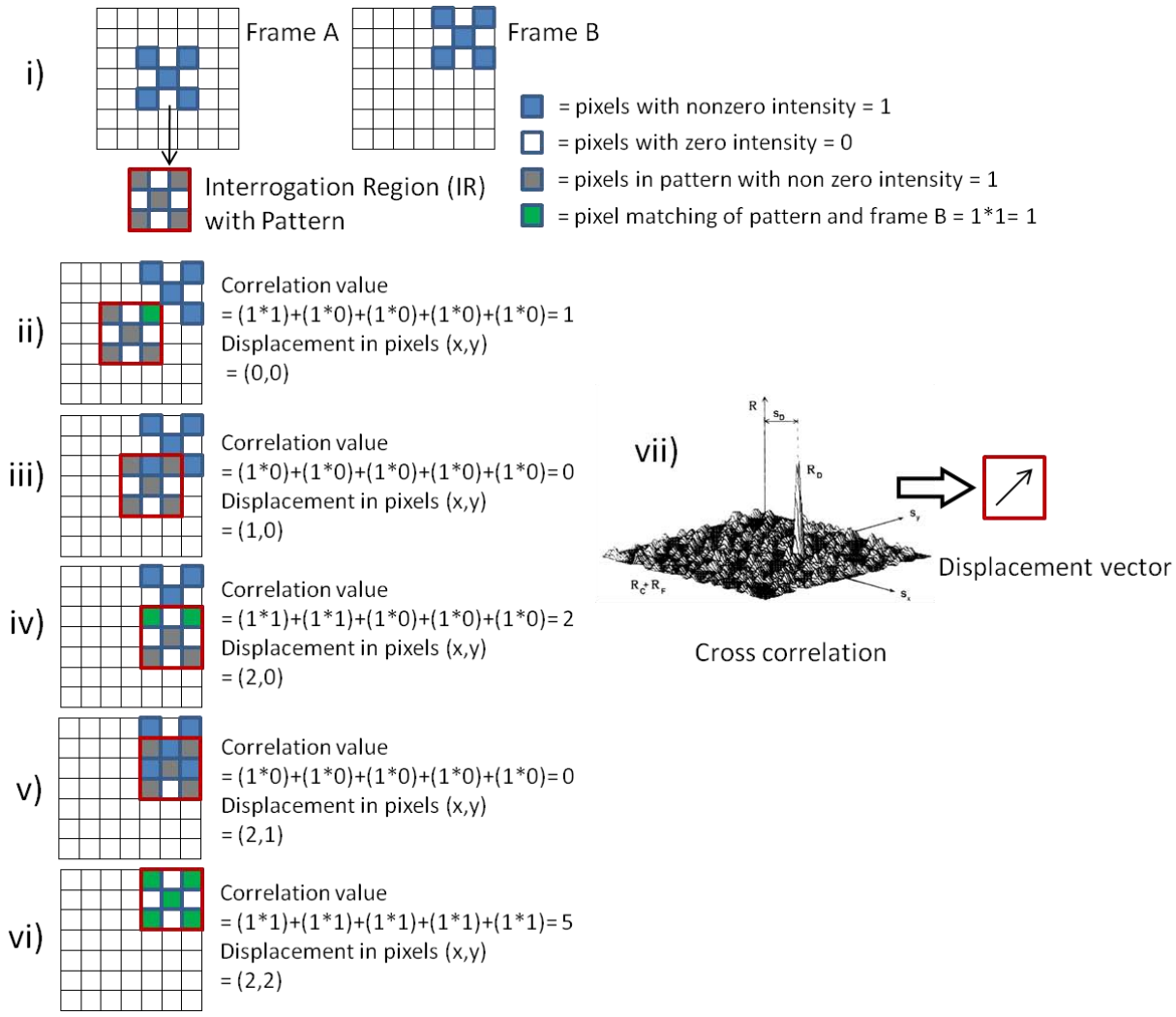

Figure 10. Example of cross correlation on digital images to obtain velocity vector [29].

Along with high speed application, PIV and PTV techniques are widely used in micro and nano level flow investigations. Boiko et al.[33] observed laminar flow separation of a quiet, laminar and low Reynolds number (Re=1060) using PIV. Koutsiaris et al. [34] used 10 µm glass bubbles to measure velocity inside 200 µm internal diameter glass capillaries using the PIV technique combined with a microscope. Lee and Kim [35] combined X-ray imaging with PIV the technique to measure velocity fields inside opaque objects. They seeded the working fluid with alumina microspheres to measure flow inside the opaque Teflon tube. Huang et al. [36] reported

0.1 pixel error in PIV measurement and suggested implementing normalized cross-correlation to reduce errors.

In the present study of resin flow, an approach is taken to measure resin flow velocity of laminated prepreg composite during cure using PIV and PTV techniques.

CHAPTER 3

TECHNICAL APPROACH

3.1 Concept

The epifluorescence technique is widely used in PIV measurements in conjunction with a microscope. This technique uses a laser of proper wavelength and fluorescent particles introduced to resin. An appropriate cutoff filter allows the desired wavelength light emitted from the particles to pass through. Resin in a laminate is usually transparent or semi-transparent in nature. Due to the non-transparent carbon fibers, laminates become opaque. Common particles such as glass particles or bubbles placed on top of the laminate surface may not be tracked because of low visibility. Therefore, the use of fluorescent particles on the top surface of the laminate can be a better solution for tracking these particles. In autoclave processing, carbon-fiber reinforced laminates are cured with a controlled heating rate under high temperature and pressure. To apply PIV/PTV measurements combined with epifluorescence, a transparent system to contain flow, is designed and manufactured to mimic the conditions of an autoclave. The concept of the experimental setup is shown in Figure 11. A specimen containing particles on the top surface is heated and compressed with two quartz plates. Quartz is selected for this method for the following reasons:

- Due to its rigidity, quartz discs transfer the applied load to the specimen in a way that imitates the pressure during cure cycle.
- Due to its transparency, a laser beam can be easily transmitted through the quartz to illuminate the seeded particles. This transparency also allows a camera to be used to track resin flow throughout the experiment.

- Due to its low coefficient of thermal expansion, quartz has little to no effect on the resin flow.

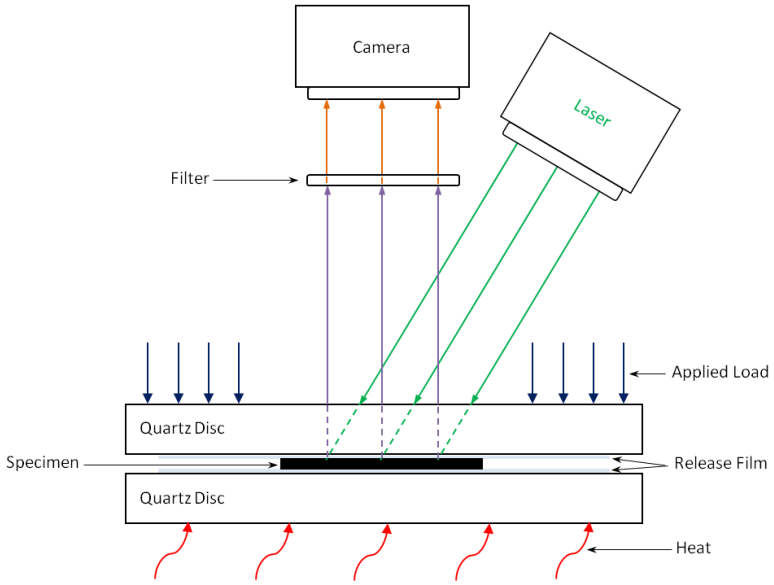

Figure 11. Concept of resin flow measurement in autoclave conditions.

Pressure on the specimen is determined by the specimen size and applied load. Details on the design and manufacture of the experimental setup, specimen preparation for various curing parameters, test conditions, and parameters for analyzing the data from the tests are given in the following sections.

3.2 Flow Apparatus and Experimental Setup

In order to obtain of resin flow velocity measurements during cure in different directions using PIV/PTV techniques, a resin flow apparatus was designed and manufactured as shown in Figure 12.

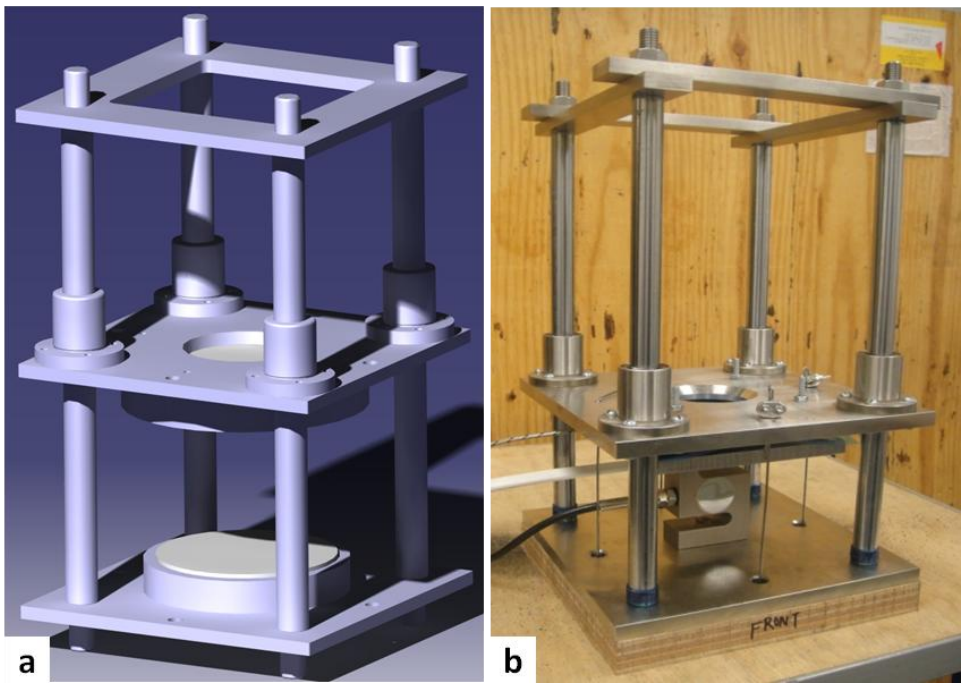

Figure 12. Resin flow apparatus; a) designed sketch b) manufactured device.

The apparatus consisted of five major units: the main structure, loading and pressure controls, heating and temperature controls, excitation, and capturing units. The main structure was made of stainless steel plates, bars, and shafts to minimize deformation of the structure due to loading and to prevent error aggravation. Dimensions of the flow apparatus are given in Table 1. The bars and bottom plate were fixed in position while the middle plate was able to move vertically. Using four shafts along with linear bearings helped keep the middle plate parallel to the bottom plate and distributed the load to the specimen uniformly. The use of linear bearings ensured that the friction forces between the linear bearings and shafts were negligible and that the load was completely applied to the specimen. A 50 mm diameter hole was made in the center of the middle plate as a window to observe the resin flow during cure. Additionally, the edge of the hole was chamfered to provide a complete side view.

TABLE 1

DIMENSIONS OF RESIN FLOW APPARATUS

Component	Dimensions (mm)	
	Length; Width; Thickness	Diameter; Length (Thickness)
Plates	200; 200; 10	
Bars	200; 25; 10	
Shafts		16; 300
Linear bearings		16; 35
Upper quartz disc		114; 6.5
Lower quartz disc		102; 6.5

Under the middle plate, the upper quartz disc (114 mm diameter) was held in position with nuts and bolts to press the specimen with the required pressure. Adequate insulation including aerogel and silicon rubber was placed between the upper quartz and middle plate to prevent the structure from heating excessively. Another quartz disc of 102 mm diameter was placed underneath the specimen to minimize the effect of thermal expansion of other parts of the structure on the resin flow. The lower quartz disc was in direct contact with a small 400W heater from the bottom to heat the specimen. To mimic the temperature change during cure cycle, a PID temperature controller with a K-type thermocouple was also attached to the apparatus near the specimen. A LabVIEW code was developed to communicate with the controller and retrieve data.

An aluminum plate placed underneath the structure was connected to the middle plate through four 3 mm diameter stainless steel rods. The desired pressure was applied to the specimen by placing specific amounts of dead weights on the aluminum plate. A load cell located between the bottom plate and heater was used to capture the force applied to the specimen. Enough insulation was placed between the load cell and heater to maintain a constant

temperature of the load cell when performing the test. The pressure was calculated by dividing the force applied by the surface area.

A class IV continuous wave green laser (532 nm) of 1300 milliwatts illuminated the fluorescent particles on the specimen surface. Unlike a regular PIV test, a 40 mm diameter laser beam at an inclination angle of 60° (approx.) with the horizontal plane illuminated the moving particles rather than a laser sheet. A 5-MegaPixel (2456×2058) CCD (Charged Coupled Device) camera with 105 mm telephoto/macro lens was installed normal to the specimen surface to capture the change of particle position and specimen size and shape during cure. The size of the camera chip was 8.5×7.0 mm with cell size of 3.45×3.45 μm. Since the camera used in the test was a 12 bit CCD camera, the intensity of the image was measured on a scale of 0 to 4095 ($=2^{12}$-1) counts. The field of view (FOV) in the experiment was 32×26 mm. A high-pass 550 nm filter was connected with the lens to protect the CCD camera from high intensity laser beam reflection. This also enhanced the difference of excited particles from background. The complete experimental setup is shown in Figure 13.

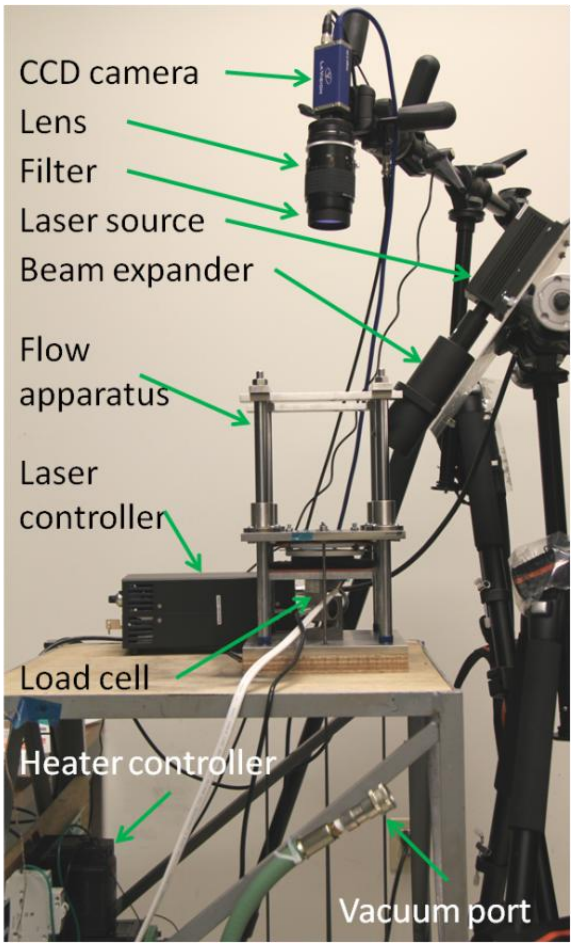

Figure 13. Experimental setup.

Two different fluorescent polymer particles were examined for the resin flow tests. The first one was a pink fluorescent particle of 20-50 μm diameter range with a density of 1.0 g/cc. The second was an orange fluorescent particle of 1-5 μm diameter with a density of 1.3 g/cc. Both of these particles, when excited by green light source of 532 nm wavelengths, emit bright orange light of 585 nm wavelengths. The melting temperature of both types was 120° C and 260° C, respectively.

3.3 Specimen Preparation

Resin flow test specimens were prepared from IM7/977-2 unidirectional (UD) and plain weave (PW) composite prepregs. The particles were first distributed on a metal surface before

being applied to the top of the composite laminate. The dimensions of the flow test specimens were 25×25mm irrespective of the material type. Typical thickness of the specimen was 1.16 mm. However, the number of layers varied with material type to achieve this thickness. Although aluminum windows were used for the resin flow test of the UD specimen, they were not used for the PW specimen.

3.3.1 Particle Distribution

After testing the compatibility of two types of fluorescent particles, only the orange fluorescent particles were used for the resin flow tests. Particle compatibility test results are provided in the results and discussion section. Orange fluorescent particles were first distributed on a solid surface before being applied to the laminate. In order to distribute particles on a solid surface, they were mixed with isopropanol (2mg particle in 150ml isopropanol) and sonicated for 10 minutes. This mixture was then sprayed under 137.9 kPa (20 psi) pressure on a 80°C 300×300 mm aluminum surface sanded with 600 grit sandpaper to obtain the correct particle distribution. As PTV analysis requires sparser particle distribution than PIV analysis, 20 ml of the above produced mixture was diluted with isopropanol to 100ml (0.27 mg/100 ml) and sprayed on a surface fitting the same specification stated above.

3.3.2 Unidirectional Specimen

Resin flow test specimens of 977-2 UD were made from eight plies of prepreg laid in fiber direction. An aluminum window dam with a thickness of 0.45mm was placed with the edges parallel to the fiber direction to prevent the fibers from spreading in a transverse direction. Figure 14 shows the complete specimen made from 977-2 UD carbon fiber epoxy composite. Although specimens were comprised of eight layers to allow for the thickness of the aluminum

dam so that the applied load acted completely on the specimen, only the top layer contained the particles.

To apply particles to the surface, laminates of 977-2 UD were uniformly pressed (approximately 1N force) against the plate where particle distribution was made. Specimens containing particles were then placed inside the aluminum window attached with a 120×120 mm release film. The aluminum window had a V notch near the specimen to connect the K-type thermocouple, as shown in Figure 14. Placing the thermocouple near the specimen ensured that the temperature cycle was applied on the test surface. Another piece of release film of the same size covered the back of the laminate to complete the test specimen.

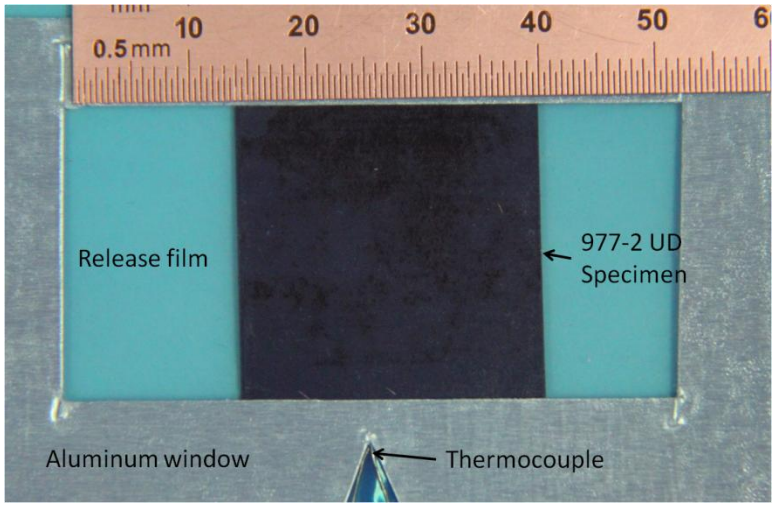

Figure 14. 977-2 UD resin flow test specimen.

The specimen preparation described above was used for the specimen subjected to test conditions of 2.8 °C/min with a 356 N load and variations in heating rate, pressure, and isothermal temperatures. Details of the test parameters are described in the test conditions section. For the resin flow test under vacuum, the laminate containing fluorescent particles was sealed inside a release film packet using rubber sealant and flash breaker tape. To distribute the vacuum pressure inside, glass fiber strings were placed around the specimen. As shown in Figure

15, an extended connection from the release film packet connected it to a vacuum port for applying vacuum during the test. Vacuum pressure (gage pressure) of -76.2 kPa was achieved during the test from the arrangement shown in Figure 15. The extra length between vacuum port and specimen packet eased the placement of specimen in the flow apparatus.

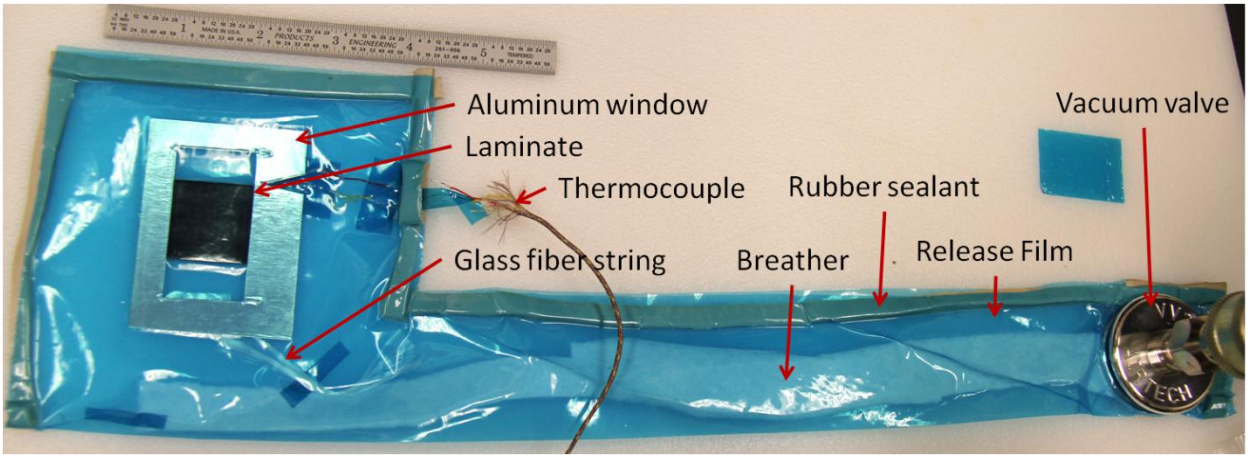

Figure 15. UD resin flow test specimen under vacuum.

3.3.3 Plain Weave Specimen

The plain weave specimen made from IM7/977-2 PW had dimensions of 25×25 mm with a typical thickness of 1.16mm. Specimens had particles distributed on their top surface. Since, the PW lamina was almost twice as thick compared to UD plies, 4 layers of PW were laid for specimen preparation. Due to the waviness in fiber tows, PW laminates were less prone to fiber wash. Hence, no aluminum window was placed around the specimen in the experiment. Figure 16 shows the complete 977-2 PW specimen. The thermocouple was attached with the top release film near the edge of the specimen as shown in Figure 16.

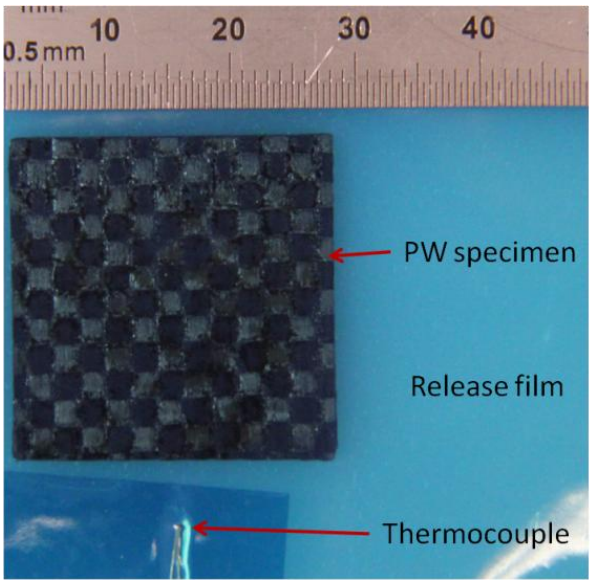

Figure 16. PW specimen for resin flow test.

3.4 Test Conditions

Resin flow tests were performed at a rate of 2.8°C/min from room temperature (23°C) to 177°C under 350 N load on IM7/977-2 UD and IM7/977-2 PW laminates. Figure 17 illustrates the temperature and pressure cycles applied during test. As the thermocouple was placed near the specimen, it was assumed that the thermocouple followed the temperature of the entire specimen. The camera and laser had fixed positions with respect to the flow apparatus. Images were taken at 30 second intervals for 60 minutes. During the test, lens aperture was kept fully open and exposure times for both camera and laser were 20ms. A programmable timing unit (PTU) was employed to control the camera exposure, maintain laser illumination, and record the test image.

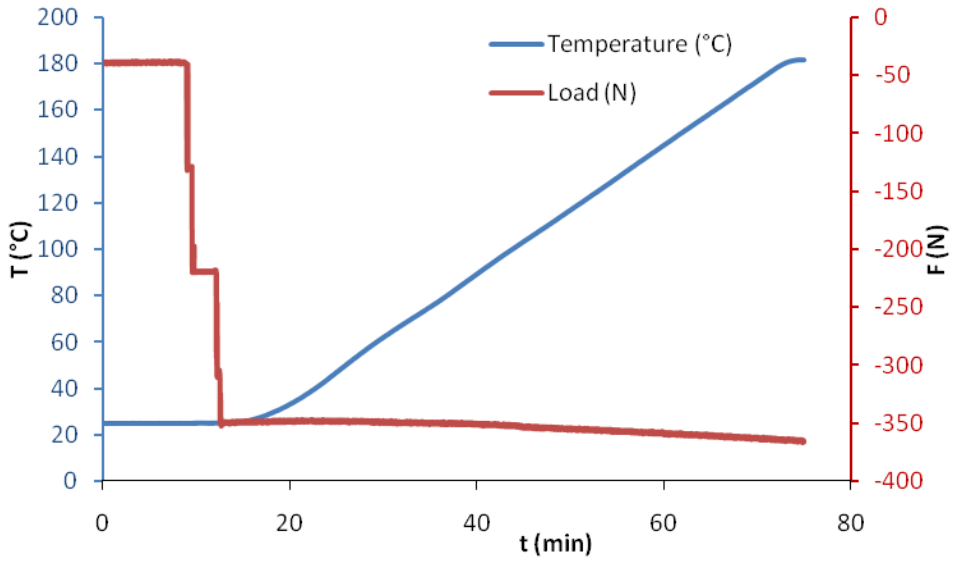

Figure 17. Resin flow test condition.

Flow tests were performed to observe the effect of various parameters of curing on the resin flow. Tests for variations of curing parameters included heating rate, pressure, vacuum, and isothermal temperature. Details of the test conditions are provided in Table 2. Unless noted, images were analyzed using the PIV technique.

TABLE 2

RESIN FLOW TEST CONDITION

Test Purpose	**Ramp Rate (°C/min)**	**Load (N)**	**Isothermal Temperature (°C)**	**Material**
Heating Rate Variation	2	356	177	8 layers of 977-2 UD
	4	356	177	
	5	356	177	
	6	356	177	
Pressure Variation	2.8	356	177	
	2.8	311	177	
	2.8	267	177	
	2.8	222	177	
	2.8	178	177	
	2.8	133	177	
	2.8	89	177	
	2.8	44	177	

TABLE 2 (continued)

Test Purpose	Ramp Rate (°C/min)	Load (N)	Isothermal Temperature (°C)	Material
Vacuum Effect	2.8	356+vacuum (-76.2 kPa)	177	
Isothermal Temperature Variation	4.5	356	70	
	4.5	356	80	
	4.5	356	90	
	4.5	356	95	
	4.5	356	100	
PTV test	2.8	356	177	
Resin Flow in PW	2.8	356	177	4 layers of 977-2 PW

Focusing of the camera was accomplished by illuminating the particles with the laser in a dark room until the camera was focused on the particles seeded on the specimen surface. While focusing was done before every test, calibration was done using a ruler of same thickness as the specimen after the test.

3.5 Analysis Parameters

During the resin flow test, correlation software Davis 8.0.6 was used to capture the images using a CCD camera through the viewing window of the flow apparatus. The same software then performed both PIV and PTV analysis between sequential images to obtain the final velocity information. PIV and PTV analysis were done on the tests performed using dense (1.33mg/100ml) and sparse (0.27mg/100ml) particle distribution respectively. Analysis steps for both PIV and PTV are briefly discussed in sections 3.5.1 and 3.5.2.

3.5.1 PIV Analysis

PIV processing was mainly comprised of two steps. First, vectors were calculated from the sequential images using cross-correlation. Next, the vector fields were processed using several filters called vector post processing to remove erroneous vectors from the vector field.

In the resin flow tests, only one camera was used to take images normal to the specimen and the time gap between each frame was predetermined. PIV analysis for the test was therefore equivalent to single frame, single exposure time series. The specimen images in the frame were geometrically masked-in to run correlation analysis. Masking of the specimen helped to reduce the analysis time as the portion outside the mask was not analyzed. Velocity vectors were calculated using the cross-correlation of sequential images. Since cross-correlation works on the interrogation region (IR) that consists of image pixels [29], multi-pass decreasing IR approach from 64×64 pixels to 32 ×32 pixels in 4 passes with 50% overlap were used for the cross-correlation analysis. Decreasing IR helped obtain better velocity gradients and ensured minimal loss of particles from the IR between two images. A 50% overlap in IR provided four times more velocity vectors than 0% overlap over the specimen surface. Vector post-processing was performed on the obtained vectors to remove outliers from the vector field. In the vector post-processing card, vector range was set to ±5 and the specified factor for the median filter was set to 1. Three passes were performed to ensure the removal of the inaccurate vectors. A detail of this option be found in the Davis Flowmaster Manual [27].

PIV analysis for the resin flow test of PW was different from the analysis procedure of UD specimens. Because of the waviness of PW, bends in tow scattered a large enough portion of laser that the filter was unable to block. As a result, high intensity light was visible on the bent. Image preprocessing was done on the test images before applying cross-correlation to obtain the vector field.

3.5.2 PTV Analysis

PTV processing had three major steps: image preprocessing, vector calculation, and post processing of the vector fields. Vector calculation itself included two sub-steps: particle detection and tracking.

The image preprocessing increased image quality by removing the background intensity. This was usually done by first subtracting background intensity that did not occur from seeding particles, then normalizing the particle intensity on the whole image and among frames. While a sliding minimum of 5 pixels was subtracted to remove back ground intensity, the intensity of the image was normalized by a sliding average over 250 pixels. All frames were normalized with respect to the first image. Normalization was necessary to work with a constant minimum intensity for particle recognition. Subtracting the minimum background of 5 pixels denotes that the local minimum intensity over 5×5 pixels is subtracted.

For vector calculation, the particle image intensities were set to a minimum intensity value to detect the pixels as particles. Pixels with intensities less than the set value were discarded. These particles were then searched in the sequential images over a fixed search area of the next image to get the velocity vectors. The search area was determined by limiting the allowed velocity range. For resin flow PTV analysis, the particle intensity threshold was 550 counts and the allotted velocity range was 10 pixels/second. The vector post-processing parameters for PTV were the same as PIV analysis.

CHAPTER 4

RESULTS AND DISCUSSION

4.1 Particle Distribution

The compatibility of the fluorescent particles was checked by heating them to high temperatures. The fluorescent particles embedded in the bulk resin were heated to 180°C from room temperature at a rate of 2°C/min. Zeiss axiovision microscope captured the state of particles at 10X magnification while the particles were being heated. Figure 18 and Figure 19 show the results of heating pink and orange fluorescent particles, respectively.

As shown in Figure 18, the pink fluorescent particles melted gradually when the temperature rose above 120°C. The same test was conducted with orange fluorescent particles and these particles showed stability at a higher temperature (180°C). Figure 19 illustrates the stability of orange fluorescent particles at high temperature. In addition, the density of orange fluorescent particles are almost the same as the density of bulk resin in the Cytec 977-2 UD [37] material (particle and resin density is 1.30 and 1.31 g/cc respectively). Similar densities and a small particle size (1-5µm) reduced the gravitational effect on the resin flow test, shifting the settling velocity towards zero. Due to high temperature stability and negligible gravitational effect on the resin flow, orange fluorescent particles has been used in all the resin flow tests.

Figure 18. Pink fluorescent particles (20-50µm) at a) room temperature; b) 80°C; c) 100°C; d) 120°C; e) 180°C.

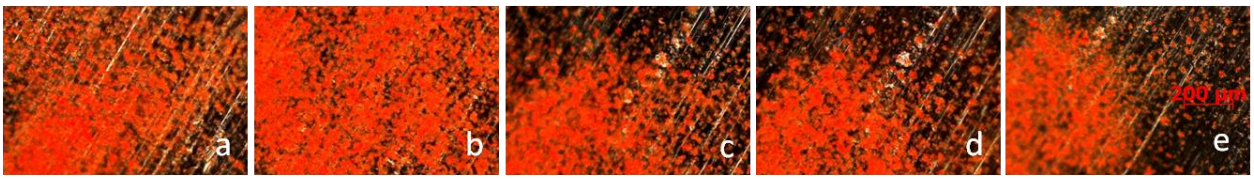

Figure 19. Orange fluorescent particles (1-5µm) at a) room temperature; b) 80°C; c) 100°C; d) 120°C; e) 180°C.

Distributions of the orange fluorescent particles on a dry, clean surface under microscope at 20X magnification are shown in Figure 20. Particles are distributed by precipitation and spraying of the particle-isopropanol mixture described previously. The particle distribution was sparser for spray distribution than precipitation distribution. Spray distribution allows for the control of the amount of particles and reduces chances of particles coagulating on the surface. Particles distributed by spraying of 1.33 mg/100 ml and 0.27 mg/100 ml particle-isopropanol mixture under 137.89 kPa (20 psi) were used for resin flow measurement by PIV and PTV respectively. Figure 21 shows the particle distribution on laminate surface taken by the CCD camera for the distribution given in Figure 20 (b,c). Separate particle images can be identified in Figure 21 (a,b) with a particle image diameter of 2 to 6 pixels. Due to the higher particle density in Figure 21 (a), some coagulation of particles is also visible. On an average seven particle images are visible in 32×32 pixel area for PIV particles distribution. For PTV, particles are sparsely distributed and further image preprocessing is performed to eliminate background intensities occurred due to laser reflection on laminate (See Figure 21 b).

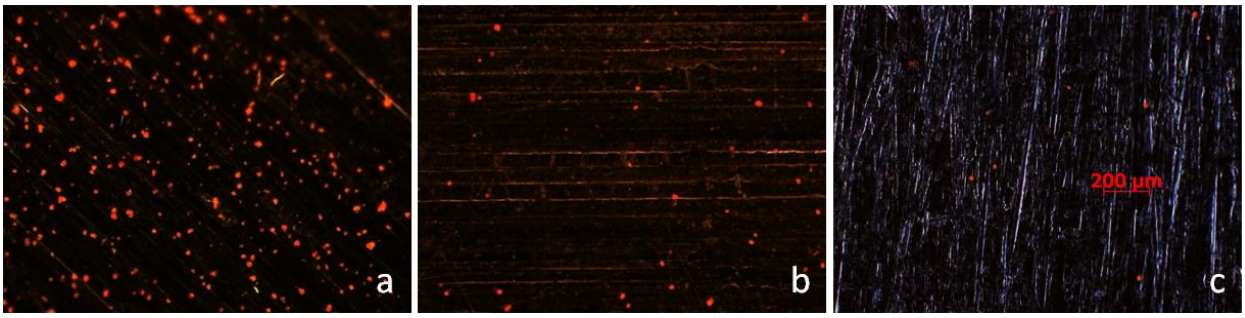

Figure 20. Particle distribution made by: a) precipitation; b) spray of 1.33mg/100ml (for PIV); and c) 0.27 mg/100ml (for PTV) particle-isopropanol mixture.

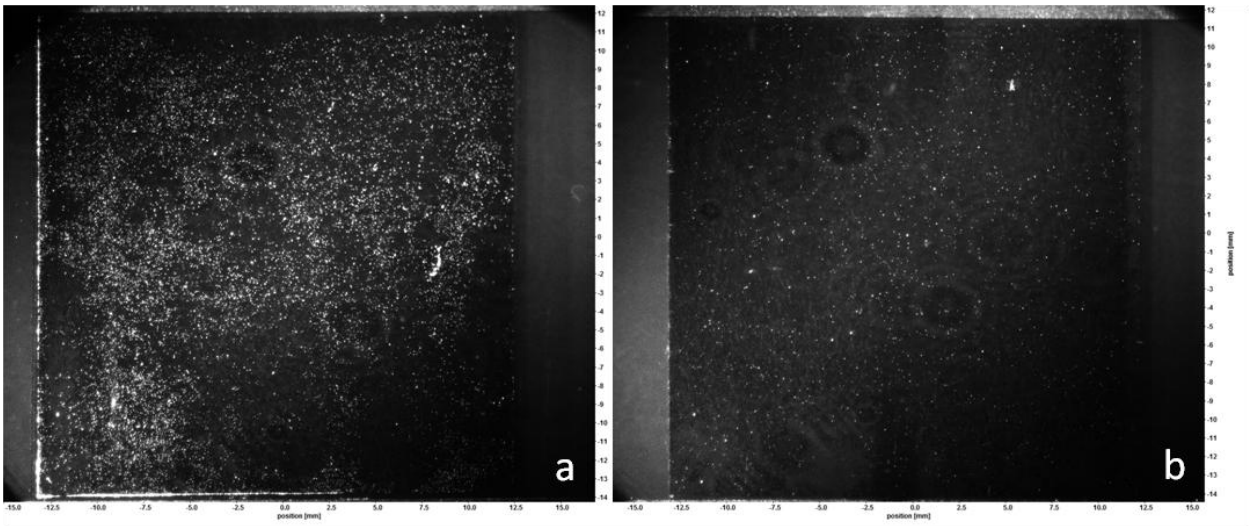

Figure 21. Filtered monochrome pictures taken by the camera that shows particle distribution on laminates a) for PIV applications b) for PTV applications.

4.2 Resin Flow Velocity in 977-2 UD

Resin flow test results of the 977-2 UD composite for varying test conditions mentioned in Table 2 are given in the following sections . Section 4.2.1 describes the resin flow results for the curing cycle given in Figure 17 which was analyzed via PIV, 4.2.2 describes the results of PTV experiment. In sections 4.2.3 to 4.2.6, the effect of heating rate, load, vacuum, and isothermal temperature on resin velocity, maximum velocity occurrence time, and flow cessation time are discussed.

4.2.1 Flow Results by PIV Analysis

The resin flow test velocity vectors and contour plots of velocity magnitude for the 3rd, 15th, 19th, 26th and 40th minute are shown in Figure 22, providing an overall view of change in resin velocity over the time during the experiment. As shown by the vector fields and contour plots, resin velocity increased from the time the experiment began until the 19th minute. After this, it decreases to cessation. Several experiments under the same test condition showed that resin movement approach cessation after 40 minutes. Therefore, the tests were conducted for 60 minutes to obtain the flow cessation time.

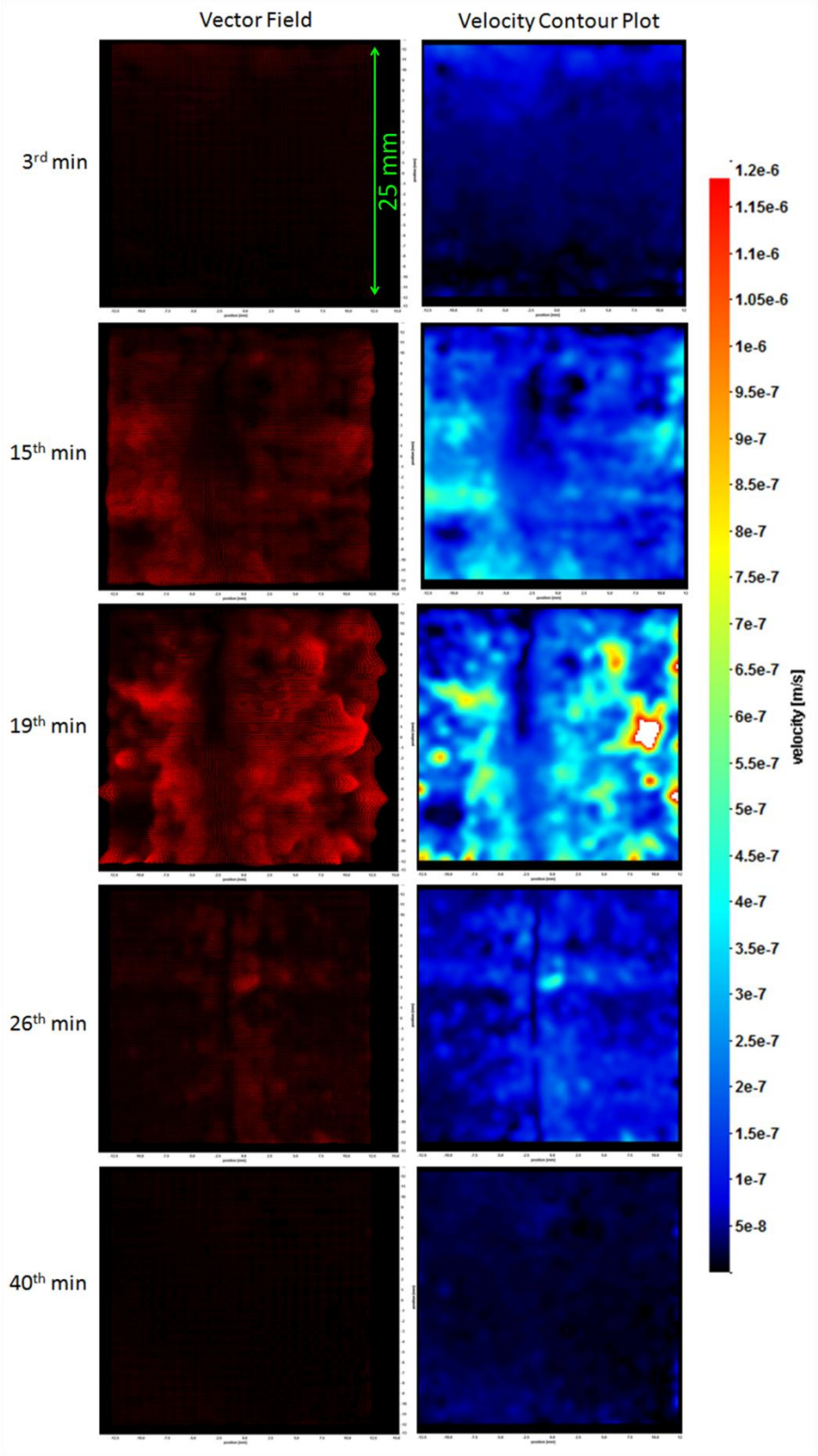

Figure 22. Velocity vectors and contour plots of resin flow test results.

The resin velocity vector field at the 19th minute of the test shown in Figure 22 is enlarged and separately shown in Figure 23. The vectors in Figure 23 are presented with 50X magnification. Figure 23 illustrates that the resin flow velocity over the specimen was non uniform in value but uniform in direction. The resin flow velocity components (V_x, V_y) at the 19th minute of the test are shown in the contour plots in Figure 24. The variation in longitudinal (V_x) and transverse (V_y) velocity over the specimen coordinate showed a non-uniform distribution. In Figure 24 (a), higher values of V_x occurred near the free edge as well as in the region between the center and edges of the specimen. The V_x is an order of magnitude higher than V_y as shown in the scale bars of Figure 24 (a, b). Although the edges parallel to fiber direction were fixed with an aluminum dam, higher values of V_y occur near these edges as shown in Figure 24 (b). The longitudinal and transverse velocity components plotted over the specimen co-ordinates(see Figure 25 a and b), show the quantitative difference between V_x and V_y. Figure 25 and Figure 24 illustrate that, while maximum longitudinal velocity (V_{xmax}) occurred in the region between the center and free edge, maximum transverse velocity (V_{ymax}) occurred near the edge of the aluminum window. As depicted in Figure 25, at the 19th minute, V_{xmax} and V_{ymax} over the specimen were 1.47 and 0.37 μm/s, respectively.

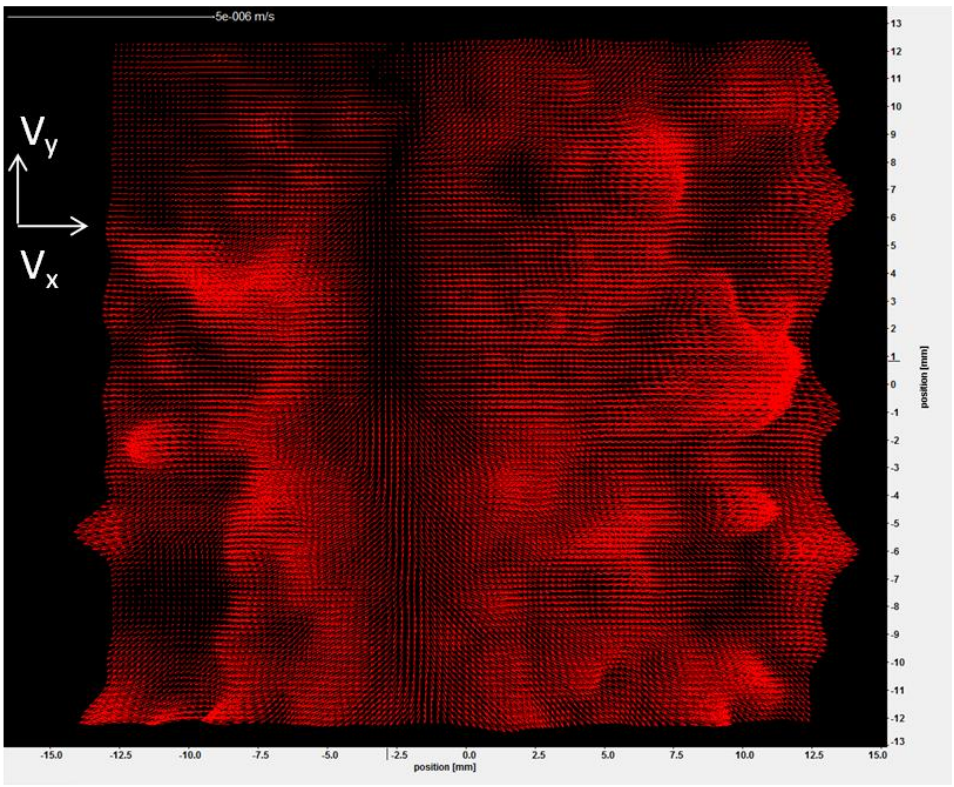

Figure 23. Resin velocity vectors magnified 50X at 19th minute.

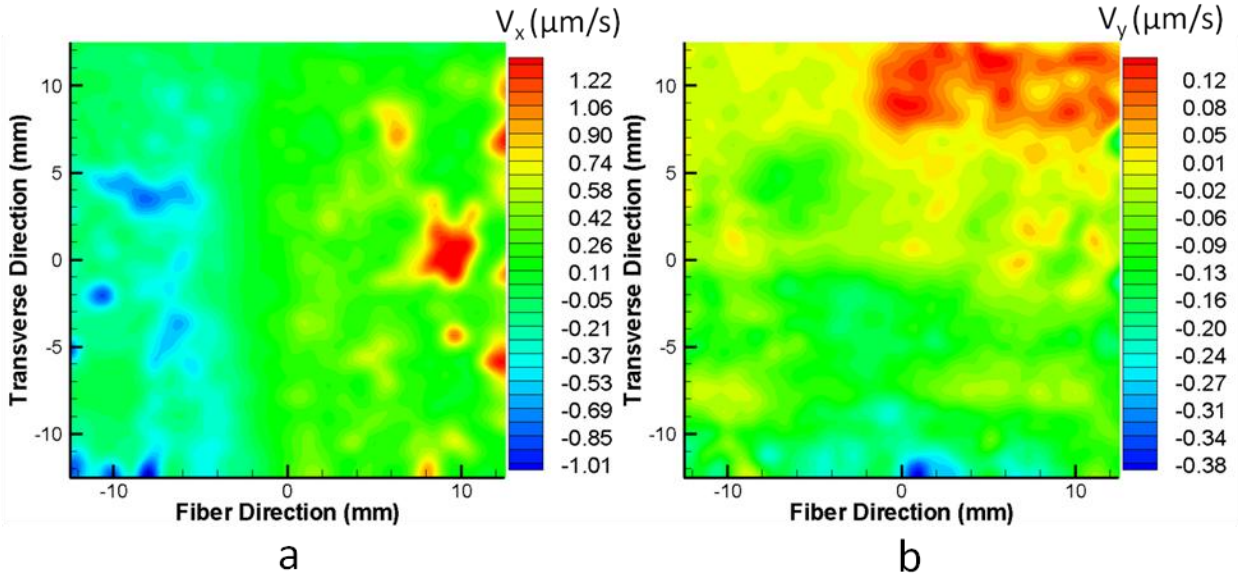

Figure 24. Contour plot of velocity components over the specimen a) longitudinal (V_x) and b) transverse (V_y) velocity.

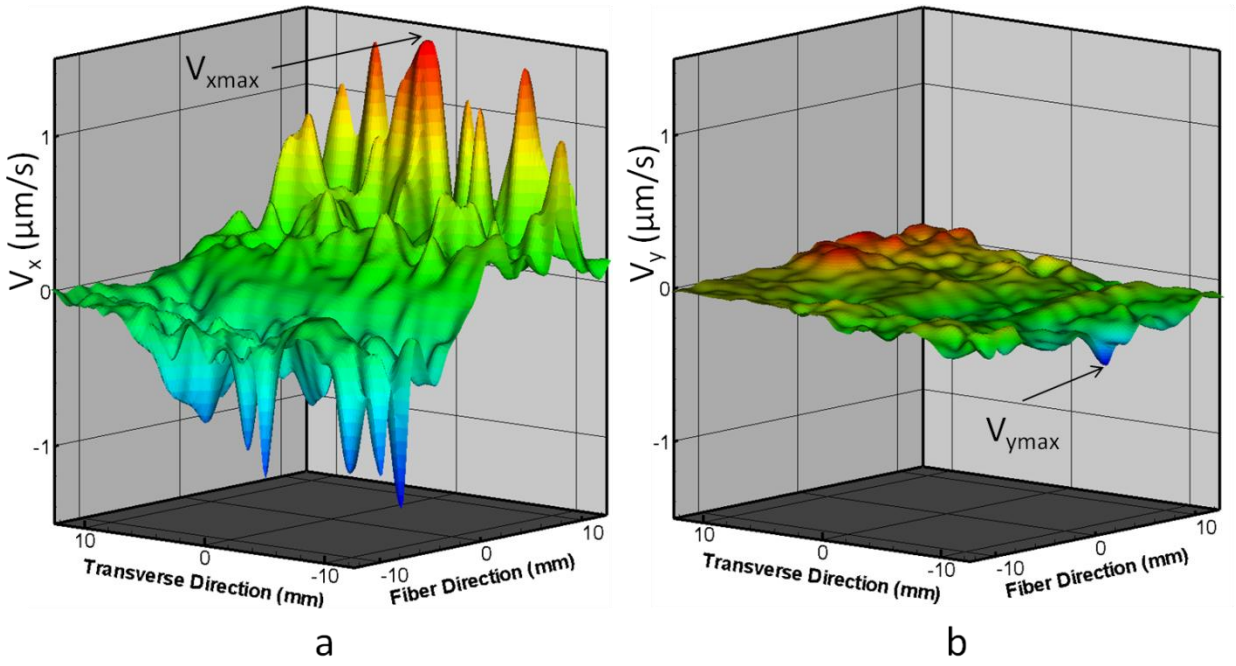

Figure 25. Resin velocity component over the specimen a) Longitudinal direction (V_x) b) Transverse direction (V_y).

As illustrated in Figure 25, both V_x and V_y over the specimen coordinates changed from point to point. Therefore, V_{xmax} and V_{ymax} of the vector fields were selected to compare the state of velocity with time. To observe the change in V_{xmax} and V_{ymax} over the specimen with time during cure, these components were collected from each vector field and plotted with time. Figure 26 illustrates the change in V_{xmax} and V_{ymax}, collected from each vector field during the resin flow test. Both V_{xmax} and V_{ymax} curves with time showed waviness and therefore a smoothing on these data were performed for one minute interval. Figure 27 shows the curves of V_{xmax} for both raw and smoothed data. Similar smoothing was done for V_{ymax} and the smoothed data for both V_{xmax} and V_{ymax} with time is shown in Figure 28. As observed from Figure 28, both V_{xmax} and V_{ymax} increase with time, reach a peak value, then decrease. Some irregularities can be attributed to the resin viscosity and compaction of the fiber bed. Initially (comparatively at higher viscosity) V_{ymax} is greater than V_{xmax}, but as viscosity decreased, V_{xmax} surpassed V_{ymax}. In the early stages, fibers tended to move inside the inter fiber spaces and into the tolerance zone

between the laminate and aluminum window due to an applied load. As a result of transverse resin displacement, the initial V_{ymax} increased. The V_{xmax} and V_{ymax} reached their peaks at the 19th and 14th minute of the test, respectively. The peaks of the V_{xmax} and V_{ymax} curves in Figure 28 are the highest velocity components during the test and are named as the peak longitudinal (V_{xpeak}) and peak transverse (V_{ypeak}) velocity, respectively. The peak longitudinal (V_{xpeak}) and the peak transverse (V_{ypeak}) velocities obtained from the test are 1.47 and 0.5 µm/s respectively. Moreover, the vector that contains V_{xpeak} had a negligible transverse velocity component; therefore, the V_{xpeak} itself was the peak velocity of the resin. For example, at the 19th minute the V_{xpeak} was 1.472 µm/s whereas the velocity vector that held V_{xpeak} was 1.474 µm/s.

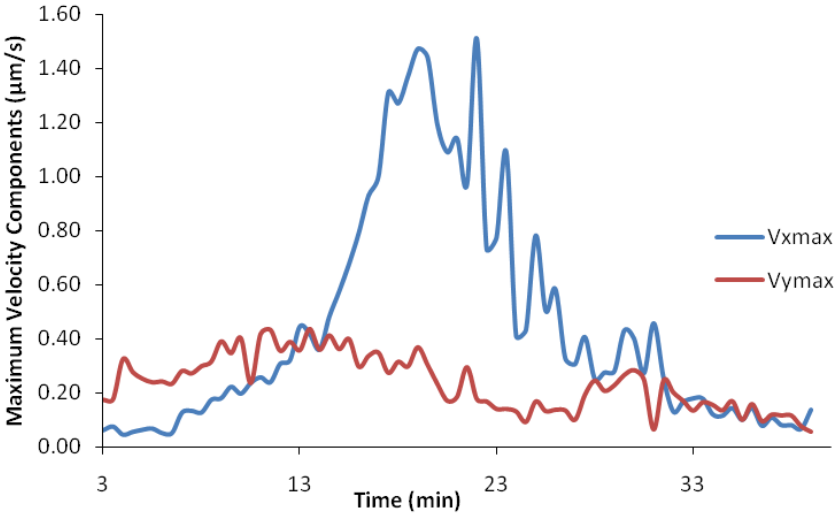

Figure 26. Maximum longitudinal and transverse velocities of the specimen with time.

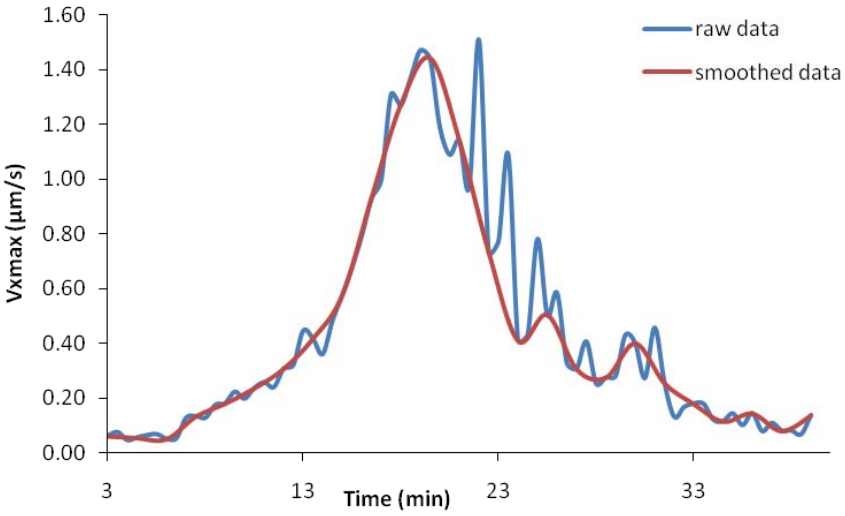

Figure 27. Smoothing of V_{xmax} with time.

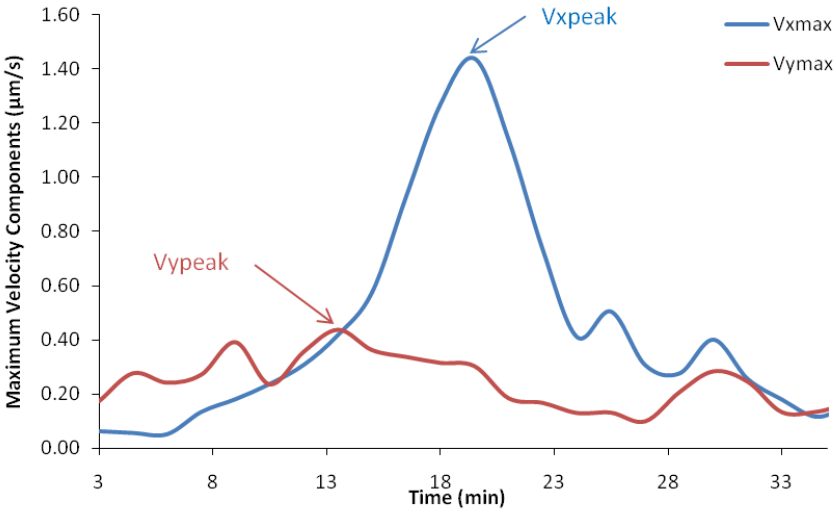

Figure 28. Maximum longitudinal and transverse velocities of the specimen with time after smoothing.

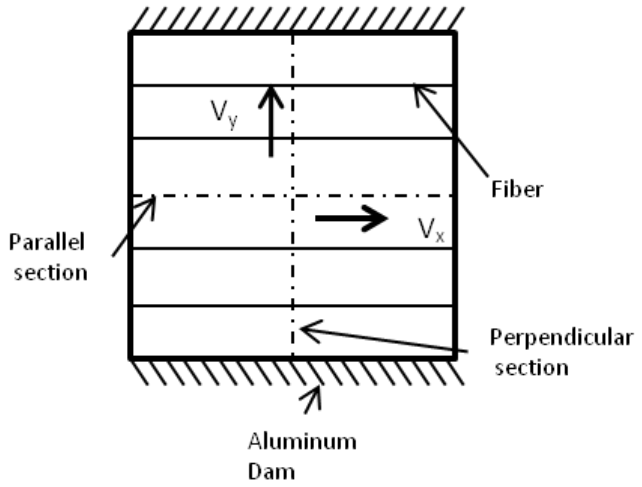

Figure 29. Flow direction and section on specimen.

An approach was taken to present the resin flow velocity over the mid sections of the specimen. The direction of the velocity components and position of the mid sections which demonstrate the resin flow velocities are shown in Figure 29. V_x and V_y are the resin flow in longitudinal (fiber) and transverse (perpendicular to fiber) directions, respectively. The mid-sections, represented as dotted lines, are named parallel and perpendicular (in regard to the fiber direction) sections. Resin velocity profiles of V_x and V_y on the parallel and perpendicular sections are shown in Figure 30 to Figure 33. For better visualization, profiles at the 3rd, 10th, 15th, 17th, 18th, 19th, 20th, 22nd, 26th, and 40th minutes are presented on these sections.

Figure 30 shows the V_x profiles on the mid parallel section. As shown in Figure 30, V_x profile on the section increased with time before decreasing to zero. The unevenness of the V_x profile can be attributed to the variation in compaction due to the waviness of the fibers in the laminate. For this particular test, V_{xmax} on the parallel section was 1.2 μm/s at the 18th minute of testing. Note that V_x shows both positive and negative values because of the opposite flow direction on the section. As seen in Figure 30, the V_x profile at the 40th minute becomes almost flat, indicating a very small resin flow or cessation of said flow. V_y profiles on the parallel

section are shown in Figure 31. Compared to the longitudinal velocity, transverse velocity was very small with a maximum value of 0.2 µm/s at the 17th minute.

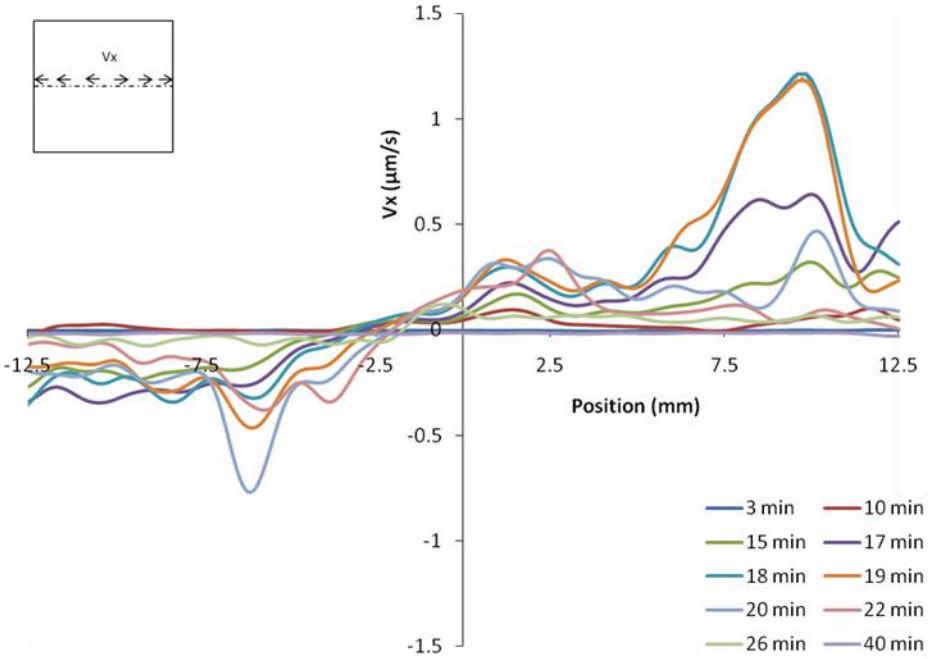

Figure 30. Resin flow in longitudinal direction on parallel section.

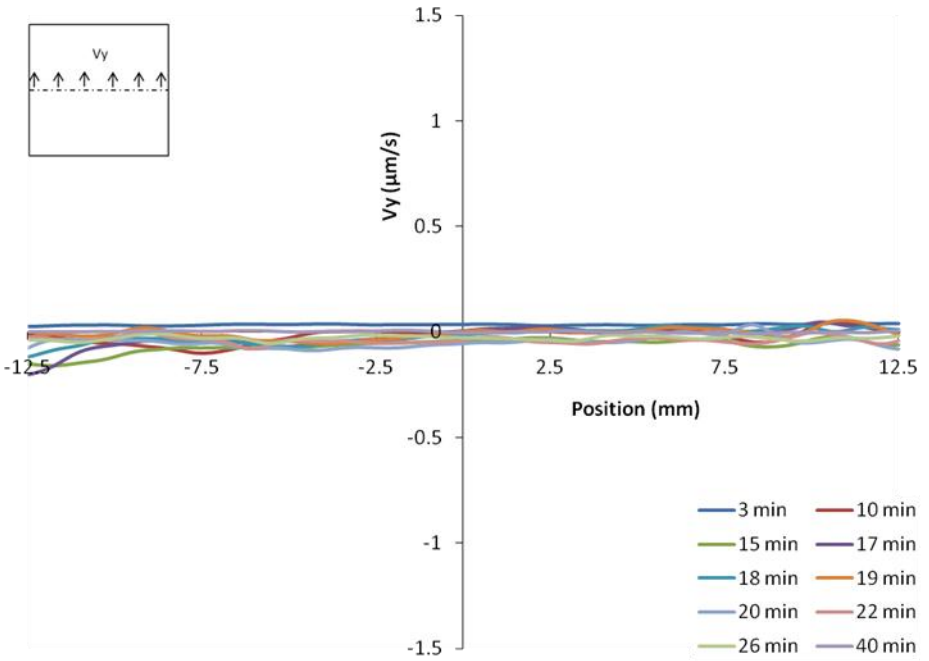

Figure 31. Resin flow in transverse direction on parallel section.

Similar to the velocity component profiles on the parallel section, longitudinal and transverse velocity profiles on the perpendicular section are shown in Figure 32 and Figure 33 respectively. While V_{xmax} on the perpendicular section is 0.5 µm/s, V_{ymax} on the same section is 0.3 µm/s. The V_{xmax} and V_{ymax} on the mid perpendicular section implies that resin velocity in the transverse direction is not always negligible compared to the longitudinal direction. On this section of the specimen, the maximum of both velocity components are small and of the same order of magnitude. V_{xmax} and V_{ymax} on the section occur at the 26th and 19th minute, respectively. Although V_{xmax} occurs at the 26th minute, the V_x profile of the 22nd minute in Figure 32 shows the larger velocity values at most of the points on the section. This situation (V_{xmax} on the section at 26th minute) may have occurred due to a change in permeability due to fiber waviness or a subtle position change of the fiber in the laminate with decreasing viscosity. The V_{xmax} of the parallel section is greater than that of the perpendicular section because of the presence of higher pressure gradients near the free edges.

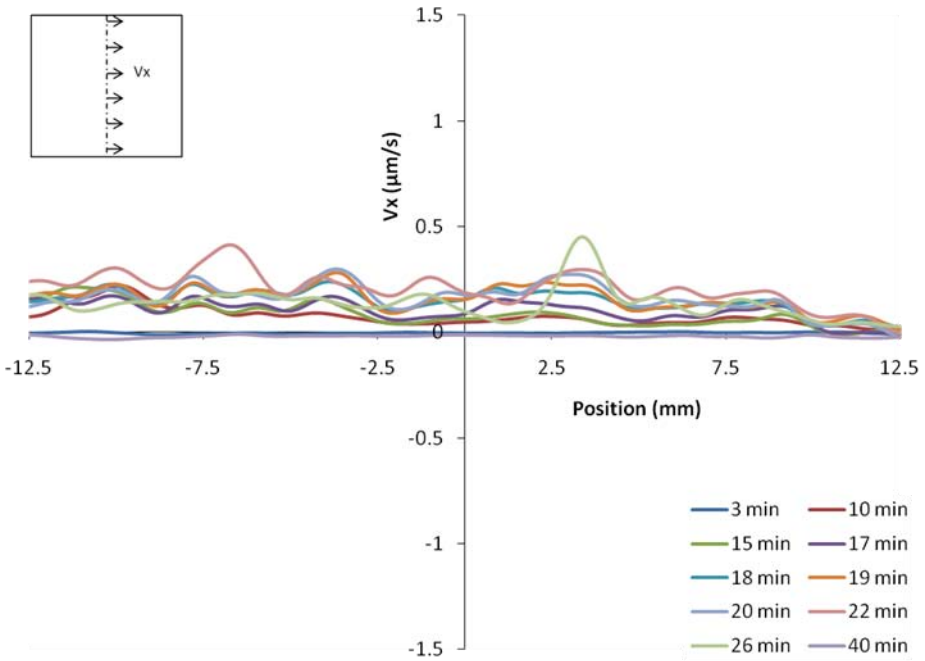

Figure 32. Resin flow in longitudinal direction on perpendicular section.

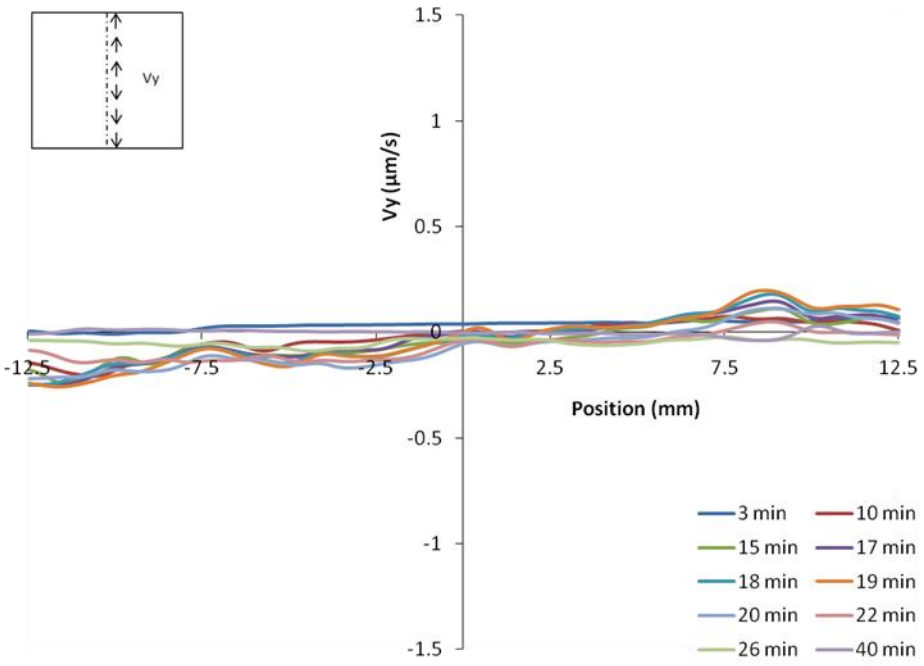

Figure 33. Resin flow in transverse direction on perpendicular section.

Observations from velocity profiles on the midsection demonstrate that V_x is greater than V_y on both sections and V_{xmax} of the parallel section is greater than that of the perpendicular section. Changes in resin velocity components (V_x, V_y) with time at 5 different points on the parallel section are shown in Figure 34 (a,b). The points chosen on the section are -10, -5, 0, 5 and 10 mm from the center of the parallel section. As seen in Figure 34, V_y is greater than V_x only at the onset of the experiment . After that, V_x becomes larger at all points until flow ceases. As observed from Figure 34 (a), resin at these points begins to move in the longitudinal direction after 10 minutes and reaches maximum velocity within 17 to 22 minutes. Longitudinal velocities at those points decrease continuously after passing the maximum velocity and become very small. When particle image displacements decrease to particle image size, velocity obtained from correlation becomes more erroneous [36]. In this situation, resin flow cessation of the specimen is determined by observing the test video. The flow cessation time is referred to as the moment from when 90-100% particles in a 7×12 mm area in the middle of the specimen stop moving.

For this experiment, the flow cessation time is recorded as the 45th minute from the start of the test.

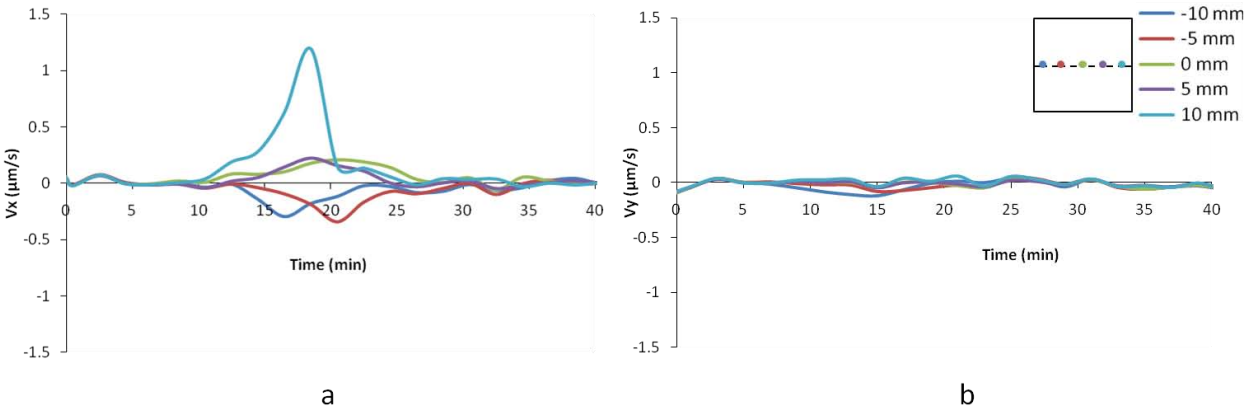

Figure 34. Resin velocity with time on parallel section a) longitudinal velocity b) transverse velocity.

Three different resin flow tests were performed under the same conditions shown in Figure 17. The average of peak velocity components of the tests (V_{xpeak} and V_{ypeak}) are 1.44 and 0.57 µm/s in longitudinal and transverse direction respectively as shown in Figure 35. Figure 36 shows the average maximum velocity components (V_{xmax} and V_{ymax}) observed on the parallel and perpendicular mid-sections. As shown in Figure 36, the average V_{xmax} and V_{ymax} on parallel sections are 1.15 and 0.28 µm/s and on the perpendicular sections are 0.46 and 0.52 µm/s respectively. As illustrated in Figure 36, average V_{xmax} is smaller than V_{ymax} in the perpendicular section. This can be caused by two factors: the pressure gradient and compaction. Although resin at points on the perpendicular mid-section carried a higher pressure than the other points on the laminate plane at any time during cure [6, 10], pressure gradients in the fiber direction at those points are lower than that near the edges. For this reason, Dave et al. [10] provides zero resin velocity at these points (perpendicular mid-section) as shown in Figure 6 (a). In this study, a small V_x is observed in the test. Moreover, when the fiber bed consolidates, fibers tend to move

inside the laminate, causing sidewise movement of fibers, resin and particles. Furthermore, the tolerance between dam and specimen edge can increase the lateral movement.

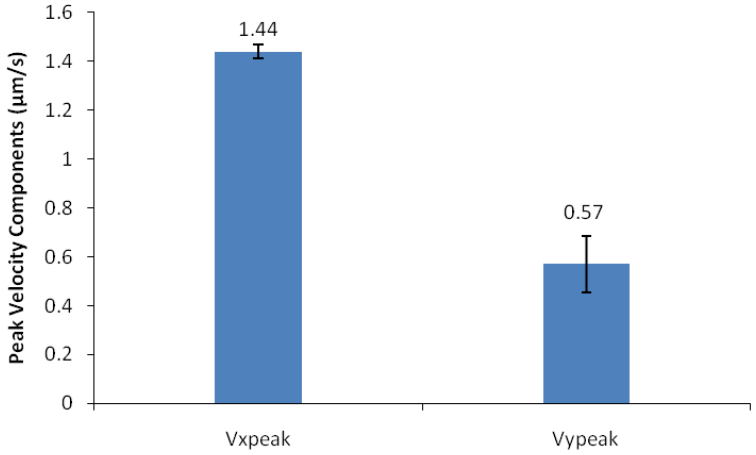

Figure 35. Average of peak velocity components (V_{xpeak}, V_{ypeak}).

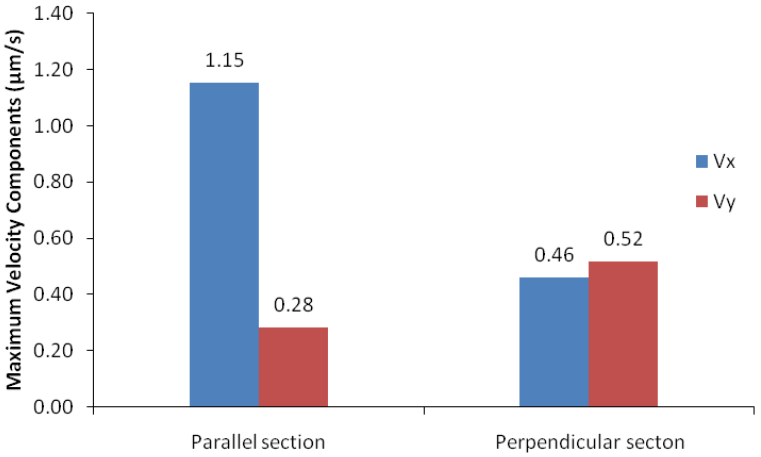

Figure 36. Maximum longitudinal (V_x) and transverse (V_y) velocities on the parallel and perpendicular section.

Since the peak longitudinal velocity (V_{xpeak}) of any test is the highest velocity component that varies with the change in curing parameters, V_{xpeak} and its occurrence times are used to describe the resin flow behavior. Again, it has been shown that V_{xpeak} represents the peak resin velocity of the flow test. Therefore, V_{xpeak} and corresponding time are mentioned as peak velocity and occurrence time of peak velocity respectively. Figure 37 shows the average peak

velocity occurrence time and flow cessation in blue columns at the 20.33 and 45.67 minute of the test respectively. Because the temperature at the start was 23±1°C (room temperature), the temperature of peak velocity and flow cessation were calculated by adding the room temperature to the product of the heating rate and corresponding time. The calculated temperatures of V_{xpeak} and flow cessation are 79.92°C and 150.88°C respectively, shown in the red columns of Figure 37.

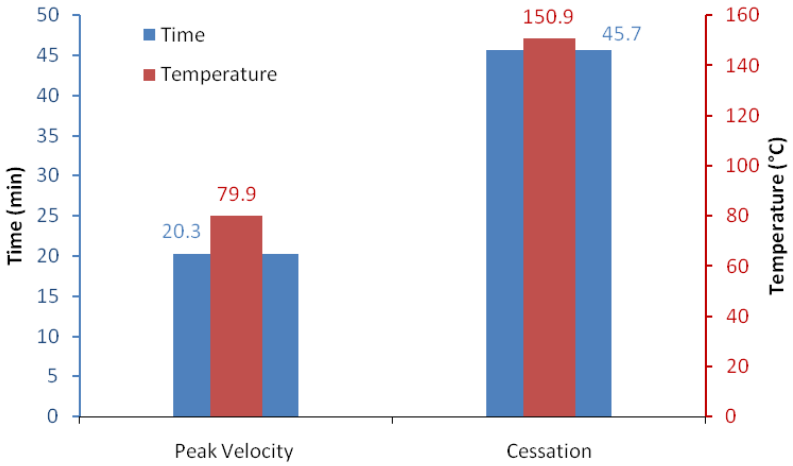

Figure 37. Time and temperature of peak velocity and cessation of resin flow.

Alavi-Soltani [25] showed the change of complex viscosity of 977-2 UD materials with time, temperature, and degree of cure using a rheometer as shown in Figure 7. He reported the average occurrence time of minimum viscosity as the 36th minute from the start of the heating which varied from 34-40 minutes. Since the ramp rate used for these tests was 2.8 °C/min, the temperature at which minimum complex viscosity occurred was between 118.2 and 135 °C. As shown in the Figure 37, peak velocity component (V_{xpeak}) occurred at an average temperature of 79.92 °C and resin flow ceased at 150.9 °C. The time of V_{xpeak} and flow cessation was 20.33 and 45.67 minutes. Hence, it can be said that maximum resin velocity occurred well before reaching the minimum complex viscosity. This phenomenon can be attributed to the combination of resin viscosity and resin and fiber pressure. In the resin flow test, heat and pressure on the specimen

were applied from the beginning. With the application of heat as viscosity decreases, resin starts to flow due to applied pressure. As the resin begins to flow, its pressure decreases [24] and applied pressure is increasingly carried by the fiber bed. With an increase in pressure on the fiber bed, the permeability of the fiber bed decreases while viscosity drop-off continues. As a result, during viscosity drop-off, resin velocity increases, reaches its peak value, then decreases again before attaining the minimum viscosity. The combination of the above-mentioned factors (resin viscosity and pressure, fiber bed pressure, and permeability) causes peak resin velocity to come earlier. Resin flow ceases after passing the minimum viscosity but significantly before reaching the gel time (77th minute of the test [25]). After passing the minimum value (resin minimum viscosity), resin viscosity starts rising and influences the flow to cease early.

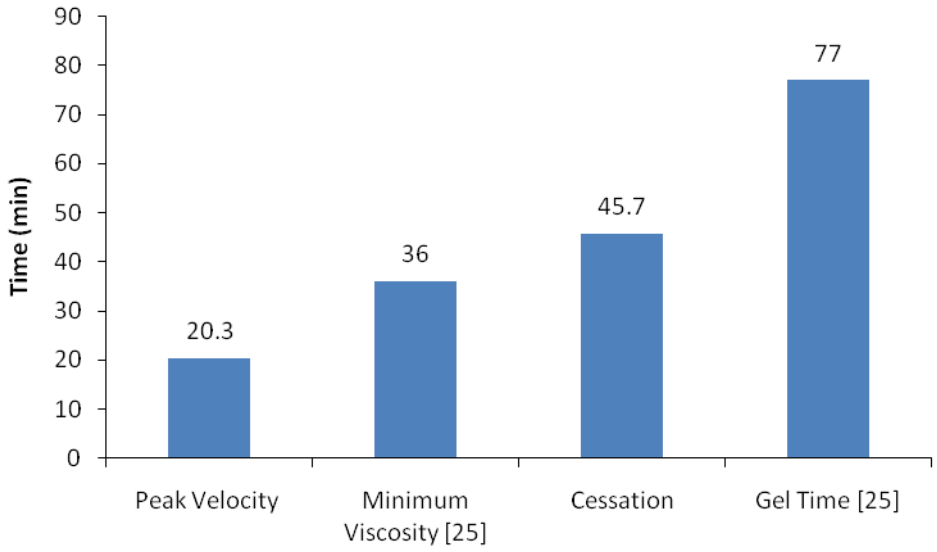

Figure 38. Comparison of peak velocity and flow cessation time with minimum viscosity and gel time.

In addition to lateral flow of resin (not fiber wash), the movement of fibers with the resin has been observed. Fiber movement occurs mainly because of a high pressure gradient on the specimen. Since fiber movement interrupts the resin flow in the test it is not desirable and was therefore, eliminated by applying a uniform load over the specimen. Figure 39 shows the result

of fiber outflow during the experiment. Due to fiber movement, resin back flow was also observed during the test.

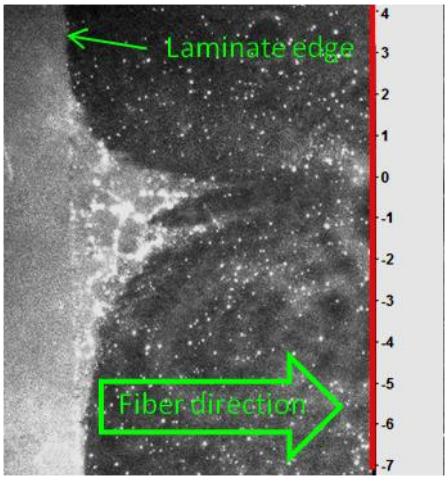

Figure 39. Observation of fiber movement.

Although resin velocity components on laminate mid-sections are obtained from resin flow tests, only the peak resin velocity (V_{xpeak}), corresponding time, and flow cessation time are considered in order to describe the effect of different parameters (temperature, pressure) on the resin flow in later sections. These components of resin flow vary with curing parameter changes.

4.2.2 Flow Results by PTV Analysis

Resin flow experiments were repeated using the PTV technique. Unlike PIV, individual particles are tracked with time to obtain velocity information. In order to facilitate particle tracking, the amount of particles was less and the particle distribution was sparser than in PIV experiments [28]. Figure 21 (b) shows the particle distribution on laminate surface for PTV measurement. Because of the nature of PTV analysis, it is not possible to obtain velocity information at every point on the specimen with time. Therefore, velocity information is available only at the points where particles are present. From PTV analysis, V_{xpeak} and V_{ypeak} are 1.5 and 0.43 μm/s occur respectively at the 18th and 15th minute. Figure 40 shows the velocity

vector field at the 18th minute. As shown in the Figure 40, particles are at the base of the instantaneous velocity vectors and the velocity directions are presented with red arrows.

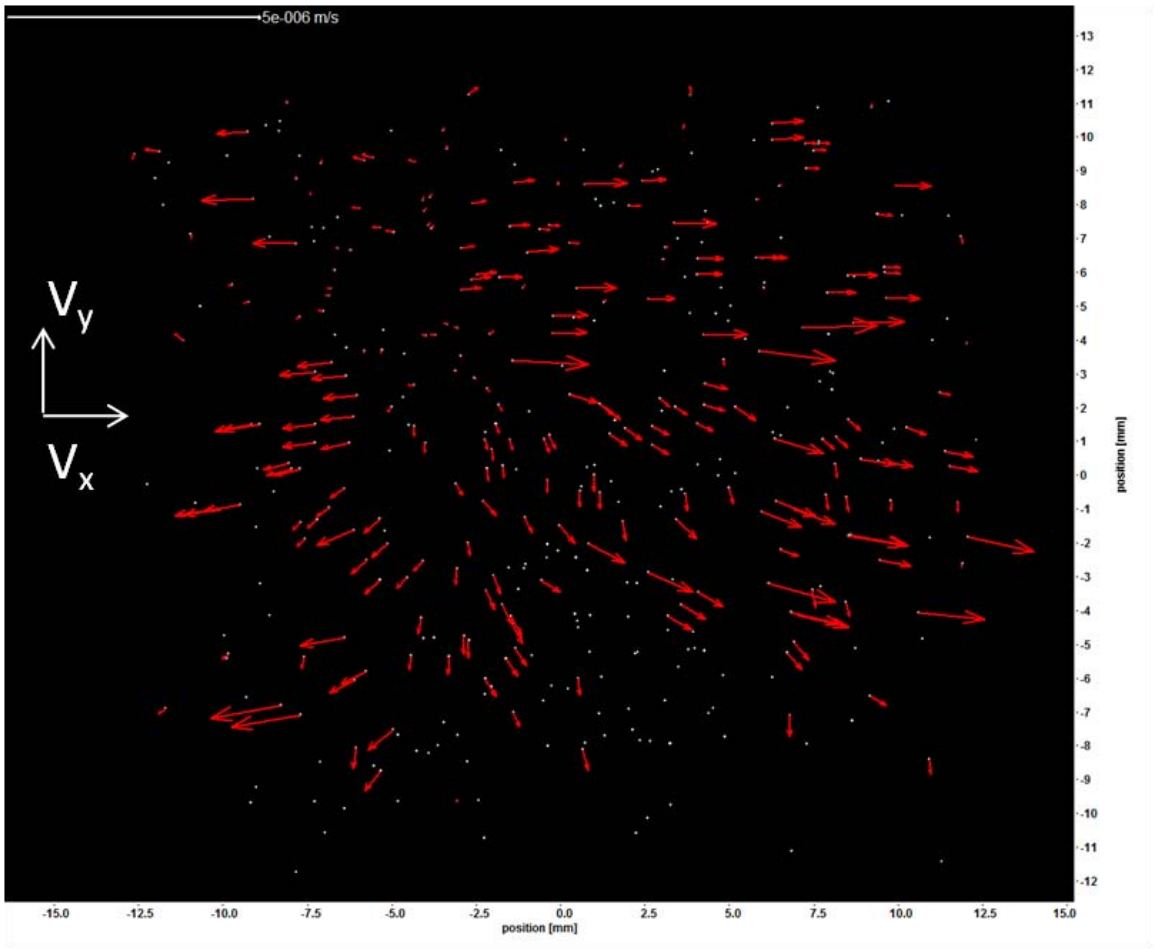

Figure 40. Velocity vector field over specimen at 18th minute (vector are 50x magnified).

In addition to velocity vector distributions over the specimen, resin flow paths are obtained from the PTV results as shown in Figure 41. Resin flow paths in Figure 41 are shown for one fourth (ex: upper-right portion of Figure 40) of the specimen. The flow path is obtained by averaging the particle movement over 10 frames. As observed from Figure 41, initially resin moved in the transverse direction before beginning to move in the longitudinal direction as the viscosity decreases. Initial lateral movement occurs as the fibers tend to move inside the lower inter fiber space in the laminate while the surface flattens due to the applied load. The upper red

box in Figure 41 shows the flow path of the resin at some position on the laminate marked by a red ellipse. After the initial transverse movement, particles move in the fiber direction as shown in Figure 41. The initial transverse movement of the particle and resin depends on the resin viscosity, inter fiber gaps in bottom fiber layers (or compaction), and pressure gradient of the resin. Again, experimental errors such as any tolerance between the aluminum dam and laminate may also affect the resin flow path and resin velocity.

Figure 41. Resin flow path.

4.2.3 Effect of Heating Rate on Resin Flow

The heating rates were varied from 2 to 6 °C/min while other parameters remained constant. The parameters of the tests are given in Table 2. The peak resin velocities (V_{xpeak}) for different heating rates are shown in Figure 42. As shown, the V_{xpeak} increases continuously with increased heating rate. For changing the ramp rate from 2 to 6 °C/min, a 60% increment in V_{xpeak} is observed. Previously, it has been observed that for a heating rate of 2.8 °C/min with 356 N

load, V_{xpeak} occurred earlier than reaching minimum viscosity time. This is attributed to the balance of resin pressure decay, resin viscosity, fiber bed permeability, and compaction. For the experiments when resin is heated with faster heating rate, resin reaches to its minimum viscosity at a quicker rate [38]. When resin viscosity is directly related to the temperature and heating rate, other factors of resin flow such as resin pressure gradient, compaction, and permeability are dependent on the applied pressure, fiber volume fraction, and viscosity. Therefore, in the experiments of various heating rates with a constant applied load, resin velocity is directly affected by the viscosity, which is dependent on temperature. Hence the resin peak velocity (V_{xpeak}) changes proportionally with changes in the heating rate.

Figure 43 illustrates that the occurrence of V_{xpeak} and flow cessation decrease with an increase in heating rate. When decreasing the ramp rate from 6 °C/min to 2 °C/min, V_{xpeak} time increases by 17 minutes and flow cessation time increases by 37 minutes.

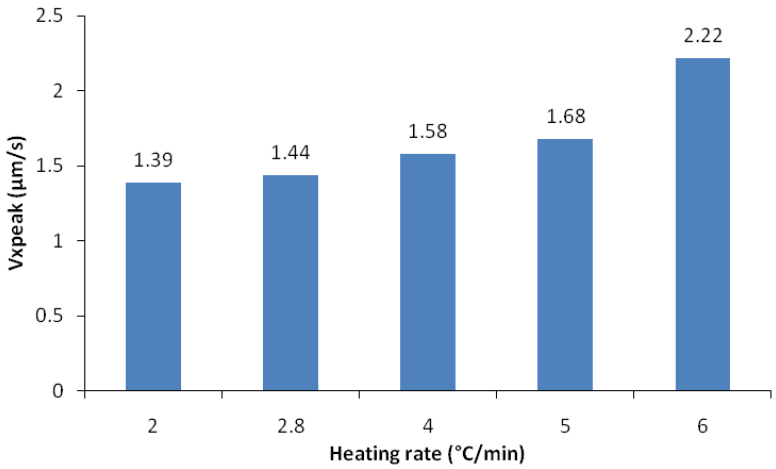

Figure 42. Effect of heating rate on peak V_x.

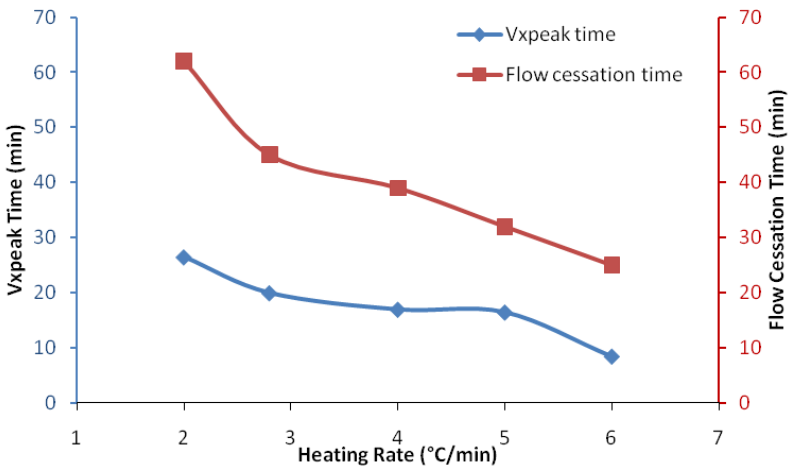

Figure 43. Flow cessation and peak V_x time variation with heating rate.

4.2.4 Effect of Pressure/Load Variation on Resin Flow

To observe the effect of load variation on resin velocity, flow tests were conducted with the same heating rate of 2.8 °C/min while varying the applied load on the specimen from 44 to 356 N. The peak resin velocities (V_{xpeak}) with various applied loads are shown in Figure 44. V_{xpeak} occurrence and flow cessation time are shown in Figure 45. As shown in Figure 45, V_{xpeak} occurrence and flow cessation time comes earlier for higher loads. Although the V_{xpeak} values in Figure 44 does not provide any direct relation to the load variation, the flow cessation time in Figure 45 shows a gradual decrease with an increase in applied load. Hence, the larger the applied load, the sooner the resin flow will terminate. As observed from Figure 45, for the applied load of 133 to 267 N, V_{xpeak} occurrence time changes very little. However, as the load is increased to 356 N, V_{xpeak} time decreases and moves downward, away from the minimum viscosity time. The occurrence time of V_{xpeak} gets closer to the minimum viscosity time when 44 N load is applied.

Although, Figure 44 does not show any relationship between V_{xpeak} and the applied load, it is obvious from this figure that the V_{xpeak} of 44 N load is greater than that of the test with 356 N load. When a larger load (356 N, for example) is applied to the specimen, resin starts moving

earlier at a higher viscosity. As the resin starts moving, resin begins losing its pressure, transferring the load to the fibers. Resin pressure loss and load transfer occurs simultaneously during the process. Therefore, a larger load causes the resin to lose its pressure faster than a smaller load as the viscosity continues to drop off. Figure 4 again illustrates a larger permeability at a lower effective load. Moreover, 977-2 UD prepregs are made of B-stage resin that has some capability to take the load at initial stages of curing when the applied load is small. Furthermore, from Figure 2, at lower effective loads (load carried by the fibers), the void ratio of the fiber bed is greater, implying that the resin volume fraction in the laminate is higher. Hence, for the test with 44 N load, the laminate contains a larger resin volume fraction and higher resin pressure near the minimum viscosity time compared to other tests. As a result, the test with 44 N load shows the largest resin V_{xpeak} near the minimum viscosity time.

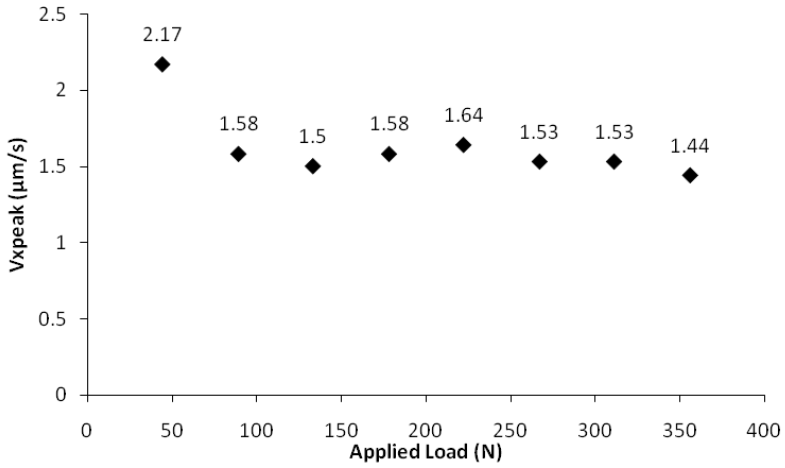

Figure 44. Peak longitudinal velocity variation with applied load.

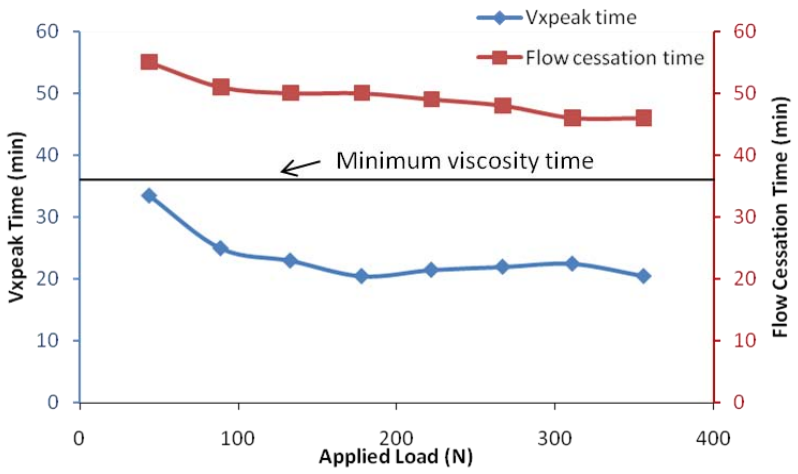

Figure 45. Variation of flow cessation and V_{xpeak} time with applied load.

4.2.5 Effect of Vacuum on Resin Flow

Figure 46 shows the peak resin velocities (V_{xpeak}) with and without vacuum. The same curing cycle as the one shown in Figure 17 was used for curing. Continuous vacuum applied during the test was -76.2 kPa (-22.5 inHg). In vacuum tests, V_{xpeak} increased by 0.57 µm/s. Both the V_{xpeak} occurrence and flow cessation time are delayed by 3.34 and 2.33 minutes respectively as shown in Figure 47. The applied vacuum creates a negative pressure on the laminate edges which pulls the resin continuously and causes the resin to move early. As the resin flows earlier, it also starts losing its pressure sooner [24] at higher viscosity. During the test, as the viscosity drops off, V_{xpeak} occurs at a lower viscosity with higher magnitude compared to the tests without a vacuum. At minimum viscosity, resin pressure becomes lesser with greater compaction. Nevertheless, resin flows mainly due to vacuum and low viscosity. It is found that at minimum viscosity (36th minute for 977-2UD [25]), V_{xmax} over the specimen with vacuum is greater than that without vacuum. The V_{xmax} at the 36th minute is 0.15 and 0.12 µm/s for the tests with and without vacuum, respectively.

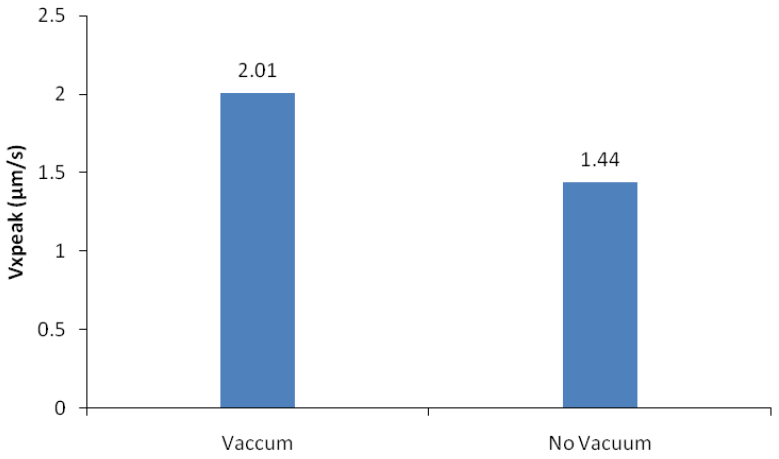

Figure 46. Effect of vacuum on peak resin velocity (V_{xpeak}).

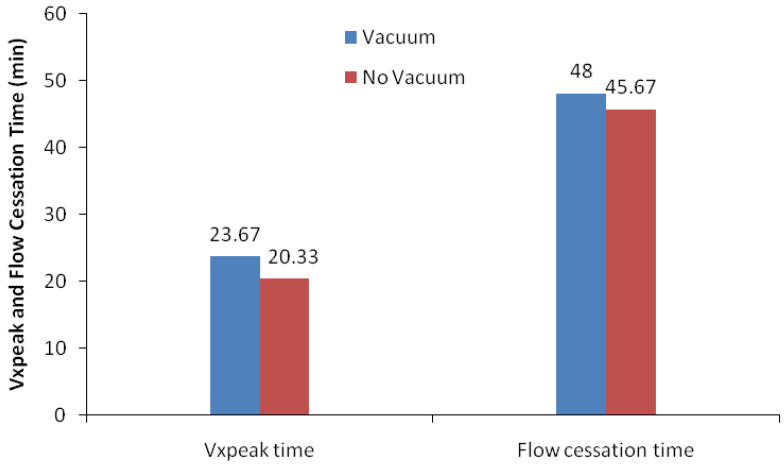

Figure 47. Flow cessation and peak V_x time variation with vacuum application.

4.2.6 Effect of Isothermal Temperature on Resin Flow

Longitudinal peak resin velocities (V_{xpeak}) with different isothermal temperatures are shown in Figure 48. The specimens were heated at a rate of 4.5°C/min to the predetermined isothermal temperatures under a 356 N load. These tests spanned 70 minutes. Figure 49 shows the V_{xpeak}'s corresponding time and flow cessation time at different isothermal temperatures. It is observed that V_{xpeak} occurrence time from attaining isothermal temperatures is inversely proportional to the isothermal temperatures itself. As analyzed from Figure 49, for the isothermal temperatures of 70, 80 and 90°C, V_{xpeak} occurs at 4, 3.8 and 1.6 minutes respectively after rising

to the isotherm. The peak velocity occurrence time from attaining the isothermal temperature decreases with the increase in temperature itself. Tests at 70, 80 and 90°C isothermal temperatures show continuous resin flow until the end of the 70 minute test. At the 100°C isothermal temperature test, resin velocity reaches its peak during heating before attaining the isothermal temperature and continues to flow until the 62nd minute.

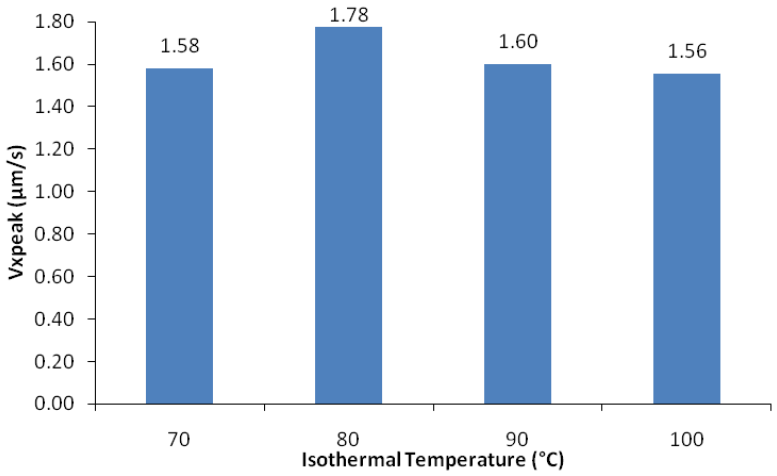

Figure 48. Effect of isothermal temperature on peak resin velocity (V_{xpeak}).

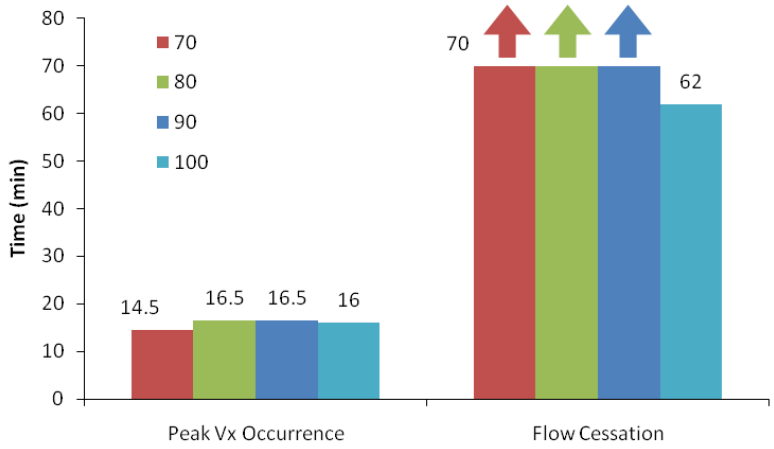

Figure 49. Flow cessation and peak V_x time variation with isothermal temperature.

The variation of V_{xpeak} with isothermal temperatures shown in Figure 48 can be explained by the changes in viscosity, resin pressure, and pressure gradient during processing. In the viscosity study of B-stage epoxy, Roller [38] observed the change of epoxy viscosity with

isothermal temperature as well as heating rate. According to his study, epoxy viscosity falls off at a faster rate with higher heating rates. During isothermal temperature, viscosity remains the same until the gelation starts at that temperature. For the 977-2 UD specimens subjected to 70, 80, and 90°C isothermal temperatures, viscosity at 70 °C is greater than the viscosity of 80 °C, which is again larger than that of 90 °C. These viscosities remain constant during isothermal temperature. Due to viscosity differences, V_{xpeak} at 80 °C is larger than that of 70 °C. Although the viscosity of 90 °C is smaller than that of 80 °C, resin pressure in the specimen at 80 °C is still comparatively greater than that of 90 °C. As it has previously been observed that V_{xpeak} occurs due to the combined effect of resin pressure and viscosity, V_{xpeak} of 80 °C is larger than that of 90 °C.

4.3 Resin Flow in 977-2 PW Specimen

The 977-2 PW specimen had very small inter tow gaps (distinguishable but not visible) where continuous lines of extra resin were present in the tow crossing zone. Measured tow width of the specimen was 2.0 mm. Resin flow tests for 977-2 PW were conducted using the cure cycle shown in Figure 17. The PW specimen for the resin flow test had no aluminum dam around it as the plain weave structure itself resisted fiber wash.

A vector field at a particular instant, superimposed on the plain weave specimen is shown in Figure 50. It shows the movement of resin in the tows and tow intersection region and illustrates that resin from each tow segment moved along the fiber direction opposite to each other and changed direction near the border of the crossing tow. Resin on the tow border moved along the edge of the tows towards the tow intersection region. These tow intersection areas are the resin rich portion of the cured laminate.

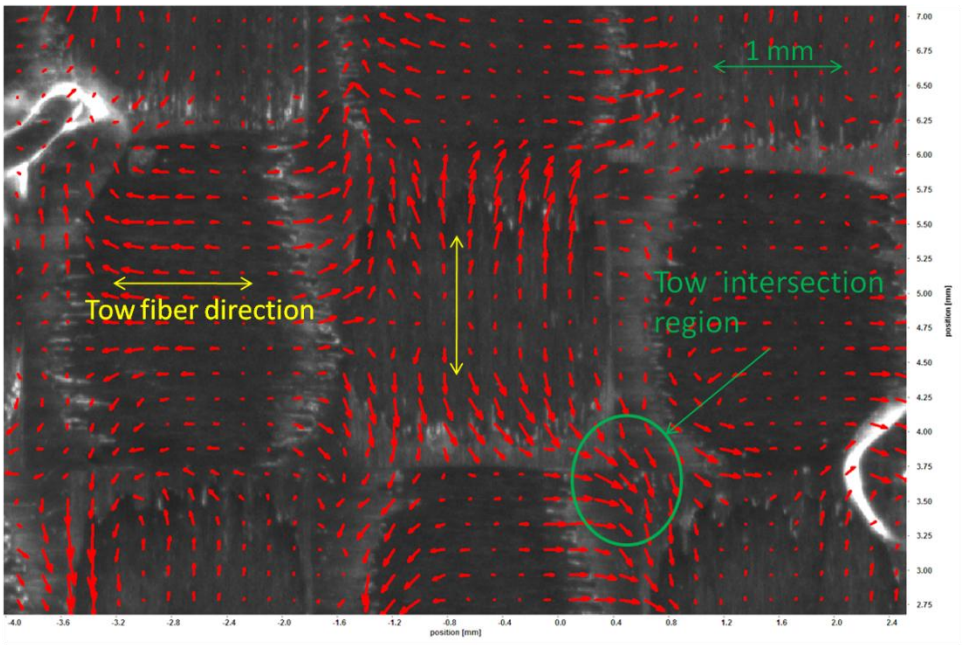

Figure 50. Velocity vector field on plain weave laminate.

Resin velocity vectors and contour plots of the 3rd, 15th, 19th, 26th and 40th minutes are shown in Figure 51. Resin flow is observed in the tow edges (inter tow space) as well as in the tow itself. Resin flow at the tow edges or borders are more dominant than the flow in the tow. During the experiment, resin may change direction in the tow intersection region or keep flowing along the tow borders depending on the local pressure gradients. The contour plots in Figure 51 show that laminate edges and the tow intersection regions exhibit higher resin velocity. From the resin flow tests of the UD specimen, resin velocity is non-uniform in magnitude, but uniform in direction. On the contrary, for the PW resin flow tests, velocity vectors are non-uniform in both magnitude and directions. A comparison of peak resin velocity components is shown in Figure 52. V_{xpeak} and V_{ypeak} of the experiment are 1.58 and 1.71 µm/s and occurred at 17th and 22nd minutes during the test respectively. As shown in the Figure 52, UD laminate longitudinal peak velocity is an order of magnitude higher than the transverse peak velocity, whereas for PW's are of the same order of magnitude. Plain weave shows higher resin velocity during cure because of

its high resin content (50% resin volume fraction in prepreg) and wider flow paths between inter tow gaps due to waviness.

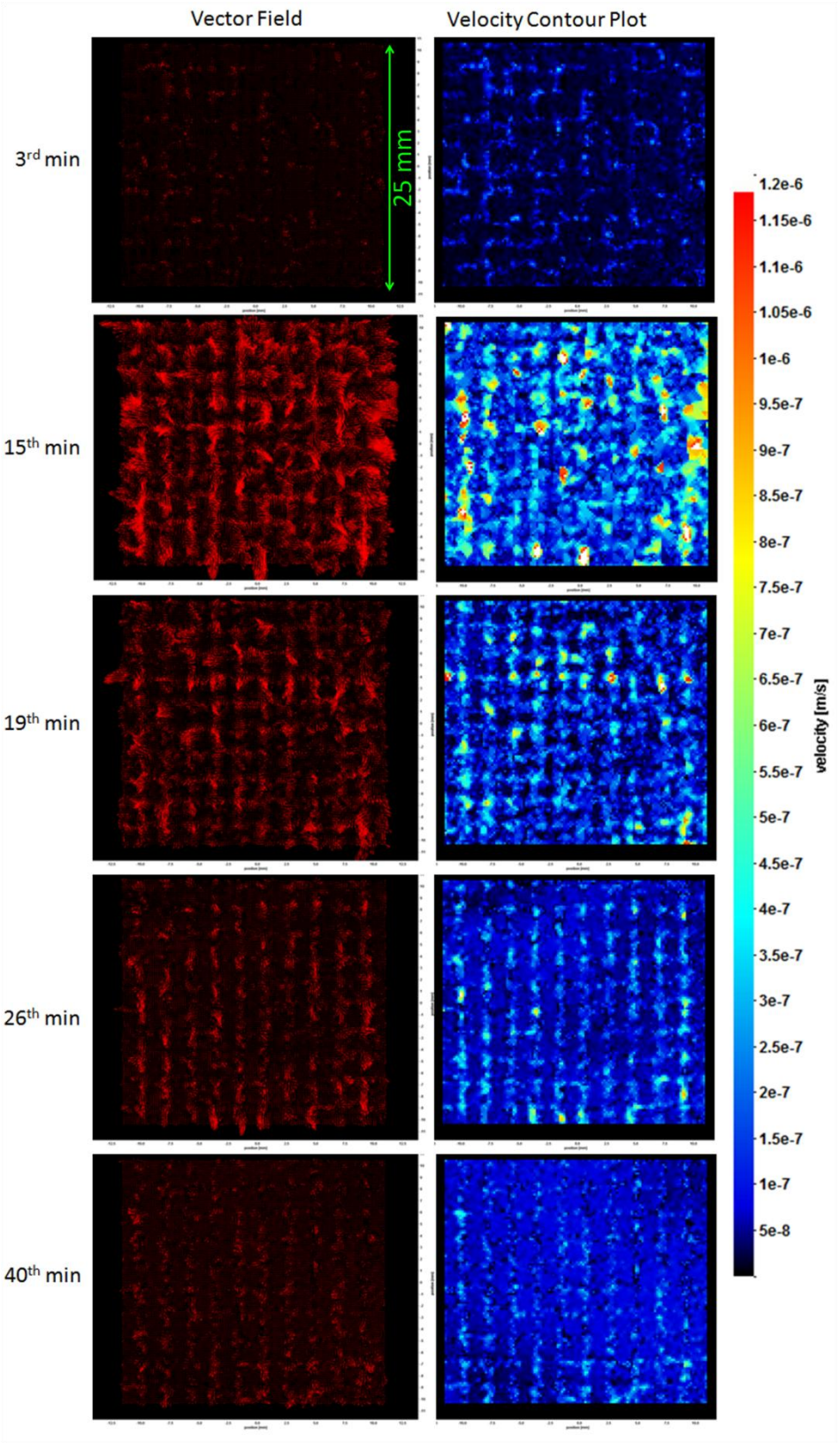

Figure 51. Vector field and contour plot of 977-2 PW laminate.

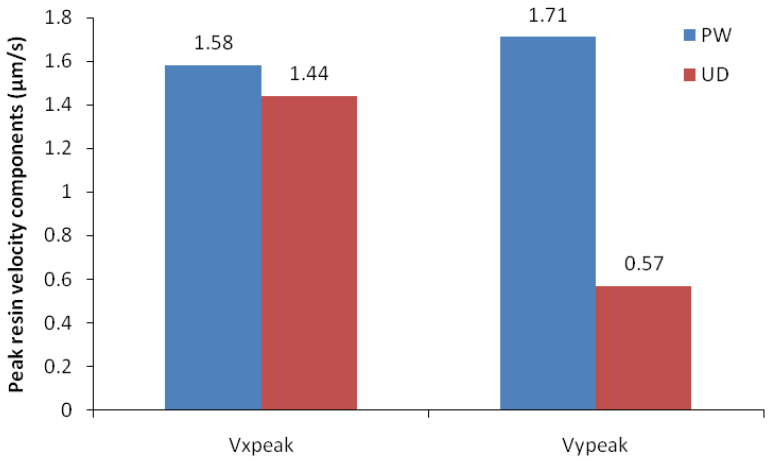

Figure 52. Comparison of peak velocity components between plain weave and unidirectional laminate.

Figure 53 (a,b) shows the longitudinal and transverse velocity profiles on the mid parallel section of the plain weave specimen. The mid sections are described in Figure 29. Due to waviness in the curves, only five velocity profiles at the 3rd, 15th, 19th, 26th and 40th minutes are shown in Figure 53. Waviness in the V_x and V_y profile of the 977-2 PW material is better understood when compared with that of the 977-2 UD. Figure 54 shows a comparison of V_x and V_y profiles between 977-2 PW and 977-2 UD specimen on the mid parallel section at the 19th minute. The waviness in the velocity component profile of PW as shown in Figure 54 occurred due to the fiber tows that cross the mid-section. As resin on each tow segment tends to move in the fiber direction opposite to each other (fiber direction shown in Figure 50), the longitudinal components showed both positive and negative values on the parallel section. The tow edges that cross mid-parallel section, causes a spiky transverse velocity profile. Due to the excess resin and less fiber to fiber contact in the plain weave specimen, resin flows until the 66th minute of the test.

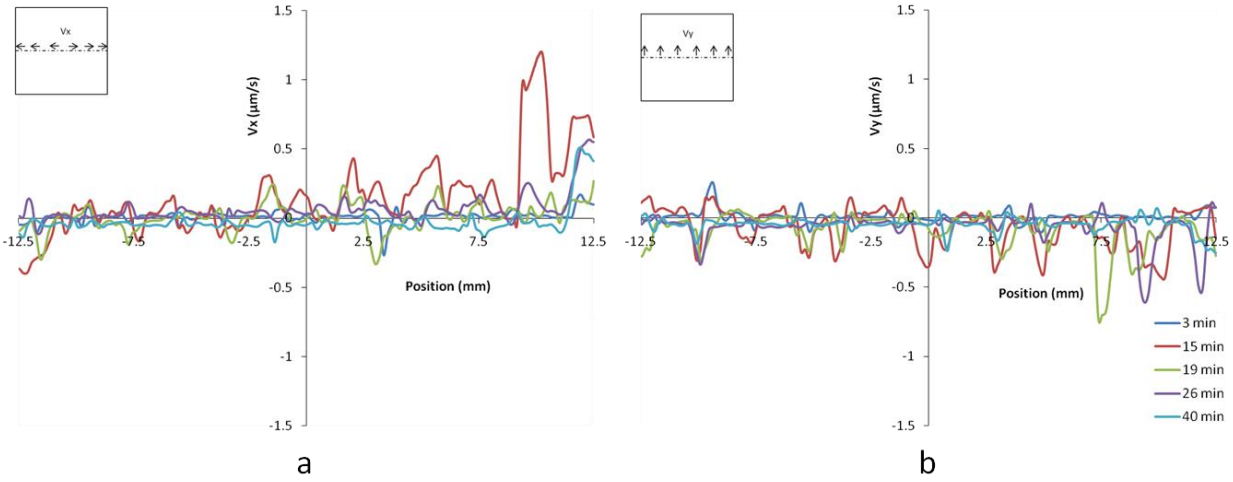

Figure 53. Resin velocity profile of 977-2 PW on parallel section in a) longitudinal direction b) transverse direction.

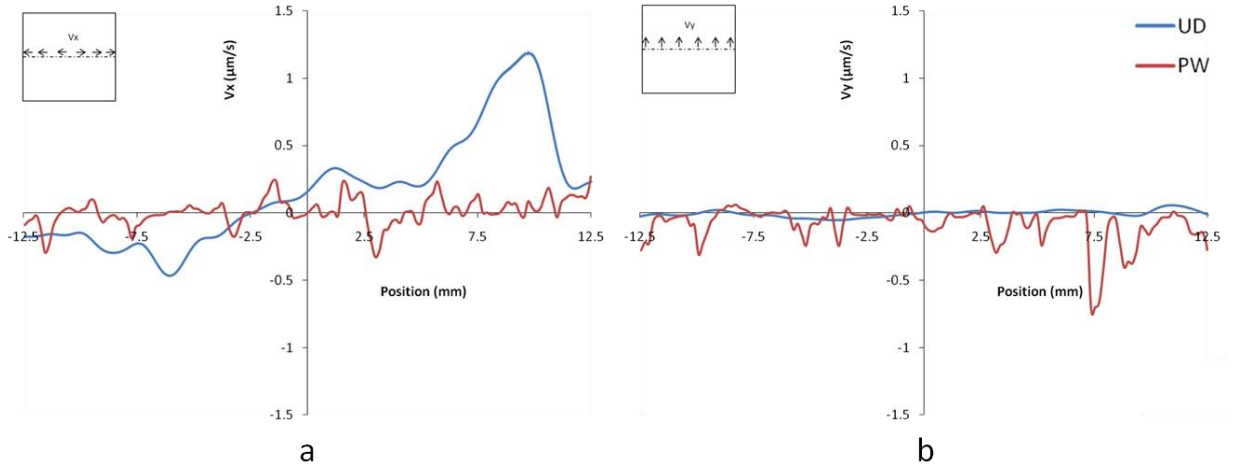

Figure 54. Comparison between 977-2 PW and 977-2 UD component profile at 19th minute a) V_x profile b) V_y profile.

CHAPTER 5

CONCLUSIONS AND FUTURE RECOMMENDATIONS

5.1 Conclusions

The main objective of this work was to study the resin flow velocity and flow pattern during autoclave processing without interrupting the cure cycle. Image correlation techniques PIV and PTV were incorporated in autoclave processing to investigate the resin flow during cure. A flow apparatus was developed to observe the resin flow while autoclave curing condition was applied on the laminate. Particles seeded on the laminate specimen were tracked during cure to obtain resin velocity over the specimen.

Suitable particles and particle distribution techniques were obtained through trial-and-error methods in the resin flow experiments. The orange polymer fluorescent particle of small diameter, high melting point and density, with a density almost equal to that of resin (particle and resin density was 1.30 and 1.31 g/cc respectively) was chosen for the flow tests. A denser and sparser particle distribution pertinent to PIV and PTV were obtained by spraying 1.33 mg/100 ml and 0.27 mg/100 ml particle-isopropanol mixture respectively under 137.9 kPa (20 psi).

In general, resin flow was transient during cure. Using the PIV technique, resin velocity components in longitudinal and transverse directions were obtained over the specimen as well as on the mid sections of the specimen. The regular curing temperature cycle with constant applied load on unidirectional laminates showed an order of magnitude higher peak longitudinal velocity than the peak transverse velocity. Experiments showed earlier resin movement in the transverse direction, but as the viscosity decreased, longitudinal velocity surpassed transverse velocity until the resin flow ceased. Observations showed that peak longitudinal velocity was the peak resin

velocity of unidirectional laminate during the flow test. The average occurrence time of peak resin velocity was approximately the 20th minute and resin flow ceased during heating stage of the temperature cycle. The resin flow in the laminates ceased after the 45th minute. Comparison of the resin flow test observations with the rheological study of 977-2 UD conducted by Alavi-Soltani [25] illustrated that peak resin velocity occurred significantly before attaining the minimum viscosity. Although the average minimum viscosity time for 977-2 UD was at the 36th minute, peak velocity occurred at the 20th minute and resin flow ceased after 9 minutes of passing minimum viscosity. The resin flow ceased before the gel time reported by Soltani for 977-2 UD (the 77th minute of the curing process).

The resin flow path was obtained by tracking individual particles using PTV analysis. Resin flow paths illustrated that initially both resin and fiber moved in the transverse direction but with time as the viscosity decreased resin started moving in the longitudinal direction. Initial transverse movement mainly occurred because of fiber rearrangement on the top laminate due to the applied load.

The effect of heating rate, applied load, applied vacuum, and isothermal temperatures were observed on resin peak velocity, corresponding time of peak velocity and flow cessation time during cure. Resin flow in the laminates were significantly affected by the curing parameters. While the resin peak velocity exhibited a continuous increase with increasing heating rate, the occurrence time of peak velocity and flow cessation time indicated a continuous decrease.

The heating rate indicated a more pronounced effect on resin flow than the applied load. Although load variation did not indicate any direct relationship with peak resin velocity,

experiments with lower loads (44 N) showed a peak resin velocity greater than the higher load (356 N). The flow cessation time showed a gradual decrease with increase in load.

It was observed that application of vacuum on regular cure cycle increased the resin peak velocity and delayed the peak velocity occurrence and flow cessation time. Lower isothermal temperatures extended the resin flow during the test. As observed from the experiments, at 70, 80, and 90°C isothermal temperatures, particle movement continued over the 70 minute test period. Moreover, at higher isothermal temperatures, resin required less time to reach the peak velocity after attaining the isothermal temperature.

The resin flow test of 977-2 PW showed the same order of peak longitudinal and transverse velocity components. Peak resin velocity obtained from the plain weave was 1.71 μm/s. Resin flow was observed in the tow, tow borders, and tow intersection region during the experiment. However, resin velocities in tow borders and tow intersection regions were greater than the velocities in the tow. The velocity vector field over the specimen showed non uniformity in both direction and magnitude of resin velocity. Velocity profiles on the mid section illustrated larger waviness compared to that of UD laminate. Because of excess resin and fiber bed structure, resin flow in PW laminate continued for a longer period compared to that of the UD laminate.

5.2 Future Recommendations

The methodology and apparatus developed in this study can be further improved by:

- Implementing automatic pressure application by a pneumatic or hydraulic system to apply pressure at a specific time during the cure cycle. The findings of that study will be pertinent to industries when analyzing resin flow for applying pressure at different times during cure.

- The quartz discs and the aluminum dam can be redesigned to estimate mass loss and thickness variation of the specimen and correlate them to the resin velocity.
- The resin flow study can be extended to measure three-dimensional velocity component of the resin flow by using stereoscopic PIV. Again, the X-ray PIV can be incorporated to measure the flow velocity inside the laminate during cure and compare it with the available resin flow results.
- A code can be developed in PIV software (Davis) to extract maximum velocity components from each vector field and plot with time to see the velocity variation with different parameters.
- Resin velocity in the specimen with larger laminate dimensions can be studied and compared with the available results.
- Using the developed flow apparatus, the mobility of the particles embedded in bulk resin can be observed to determine the minimum viscosity and gel point.
- Fluorescent nano-particles can be used to measure resin flow velocity in laminate.

REFERENCES

REFERENCES

[1] Kardos, J., Duduković, M., and Dave, R., 1986, "Void Growth and Resin Transport During Processing of Thermosetting — Matrix Composites Epoxy Resins and Composites IV," K. Dušek, ed., Springer Berlin / Heidelberg, pp. 101-123.

[2] Zhan-Sheng Guo, Ling Liu, Bo-Ming Zhang, and Shanyi Du, 2009, "Critical Void Content for Thermoset Composite Laminates," Journal of Composite Materials, 43(17), pp. 1775-1790.

[3] Tang, J. M., Lee, W. I., and Springer, G. S., 1987, "Effects of Cure Pressure on Resin Flow, Voids, and Mechanical Properties," Journal of Composite Materials, 21(5), pp. 421-440.

[4] Tavakol, B., 2011, "Prediction of Residual Stresses and Distortion of Carbon Fiber/Epoxy Composites due to Curing Process," Master of Science, Wichita State University.

[5] Berglund, L. A., and Kenny, J. M., 1991, "Processing Science for High Performance Thermoset Composites," SAMPE Journal, 27(2), p. 10.

[6] Dave, R., Kardos, J. L., and Duduković, M. P., 1987, "A Model for Fesin Flow During Composite Processing: Part 1—General Mathematical Development," Polymer Composites, 8(1), pp. 29–38.

[7] Hubert, P., 1996, "Aspects of Flow and Compaction of Laminated Composite Shapes During Cure," Doctor of Philosophy, Ecole Polytechnique de Montréal.

[8] Gutowski, T. G., Cai, Z., Bauer, S., Boucher, D., Kingery , J., and WinemanS., 1987, "Consolidation Experiments for Laminate Composites," Journal of Composite Materials 21(7), pp. 650-669

[9] Gutowski, T. G., and Dillon, G., 1992, "The Elastic Deformation of Lubricated Carbon Fiber Bundles: Comparison of Theory and Experiments," Journal of Composite Materials, 26(16), pp. 2330-2347.

[10] Dave, R., Kardos, J. L., and Duduković, M. P., 1987, "A Model for Resin Flow During Composite Processing Part 2: Numerical Analysis for Unidirectional Graphite/Epoxy Laminates," Polymer Composites, 8 pp. 123–132.

[11] Taylor, D. W., 1948, Fundamentals of Soil Mechanics, John Wiley & Sons, New York.

[12] Gutowski, T. G., 1985, "A Resin Flow/Fiber Deformation Model for Composites," SAMPE Quarterly, pp. 58-64.

[13] Bear, J., 1979, Hydraulics of Groundwater, McGraw Hill, New York.

[14] Lam, R. C., and Kardos, J. L., 1991, "The Permeability and Compressibility of Aligned and Cross-Plied Carbon Fiber Beds During Processing of composites," Polymer Engineering & Science, 31(14), pp. 1064-1070.

[15] Loos, A. C., and Springer, G. S., 1983, "Curing of Epoxy Matrix Composites," Journal of Composite Materials, 17(2), pp. 135-169

[16] Gutowski, T. G., Morigaki, T., and Z., C., 1987, "The Consolidation of Laminate Composites," Journal of Composite Materials, 21(2), pp. 172-188

[17] Smith, G. D., and Poursartip, A., 1993, "A Comparison of Two Resin Flow Models for Laminate Processing," Journal of Composite Materials, 27(17), pp. 1695-1711.

[18] Lindt, J. T., 1982, "Engineering Principles of the Formation of Epoxy Resin Composites," SAMPE Quarterly, 14, pp. 14-19.

[19] Jiang, J., Littleton, R. L., Luo, Z. P., Ellis, E. A., and Ochoa, O., 2003, "Transverse Coefficient of Thermal Expansion Determination of Carbon Fibers Using ESEM and TEM at High Temperature," Microscopy and Microanalysis, 9(SupplementS02), pp. 540-541.

[20] ASTM, 1999, "Standard Test Method for Resin Flow of Carbon Fiber-Epoxy Prepreg," ASTM D3531 -99, American Society for Testing and Materials.

[21] Poursartip, A., Riahi, G., Frederick, L., and Lin, X., 1992, "A Method to Determine Resin Flow During Curing of Composite Laminates," Polymer Composites, 13(1), pp. 58–65.

[22] Thomas, S., Bongiovanni, C., and Nutt, S. R., 2008, "In Situ Estimation of Through-Thickness Resin Flow Using Ultrasound," Composites Science and Technology, 68, pp. 3093–3098.

[23] Wartewig, S., Helmis, G., Strehmel, B., Younes, M., and Strehmel, V., 1992, "Fluorescence Probe Studies During the Curing of Epoxy Systems," Physics of Polymer Networks, Springer Berlin / Heidelberg, pp. 83-87.

[24] Mackenzie, K. A., 1993, "Measurement of Resin Pressure in Composite Laminates During Cure," Masters of Applied Science, The University of British Columbia, Vancouver, Canada.

[25] Alavi-Soltani, S., 2010, "Thermal, Rheological and Mechanical Properties of a Polymer Composite Cured at Staged Cure Cycles," Doctor of Philosophy, Wichita State University.

[26] Prasad, A. K., 2000, "Particle Image Velocimetry: Review Article," Current Science, 79(1), pp. 51-60.

[27] LaVision, 2011, FlowMaster, LaVision GmbH, Germany.

[28] LaVision, 2010, PTV, LaVision, Germany.

[29] Keane, R., and Adrian, R., 1992, "Theory of Cross-Correlation Analysis of PIV Images," Applied Scientific Research, 49(3), pp. 191-215.

[30] Raffel, M., 2007, Particle Image Velocimetry: A Practical Guide, Springer, Heidelberg; New York.

[31] Westerweel, J., 1997, "Fundamentals of Digital Particle Image Velocimetry," Measurement Science and Technology, 8(12), pp. 1379-1392.

[32] Grant, I., 1997, "Particle Image Velocimetry: A Review," Proceedings of the Institution of Mechanical Engineers, Part C: Journal of Mechanical Engineering Science, 211(1), pp. 55-76.

[33] Boiko, A., Dovgal, A., Hein, S., and Henning, A., 2011, "Particle Image Velocimetry of a Low-Reynolds-Number Separation Bubble," Experiments in Fluids, 50(1), pp. 13-21.

[34] Koutsiaris, A. G., Mathioulakis, D. S., and Tsangaris, S., 1999, "Microscope PIV for Velocity-Field Measurement of Particle Suspensions Flowing Inside Glass Capillaries," Measurement Science and Technology, 10(11), pp. 1037-1046.

[35] Lee, S. J., and Kim, G. B., 2003, "X-ray Particle Image Velocimetry for Measuring Quantitative Flow Information Inside Opaque Objects," Journal of Applied Physics, 94(5), pp. 3620-3623.

[36] Huang, H., Dabiri, D., and Gharib, M., 1997, "On Errors of Digital Particle Image Velocimetry," Measurement Science and Technology, 8(12), pp. 1427-1440.

[37] Cytec, 1995, "Cycom 977-2 Toughened Epoxy Resin," C. E. Material, ed., Cytec Engineered Material, Greenville, Texas.

[38] Roller, M. B., 1975, "Characterization of the Time-Temperature-Viscosity Behavior of Curing B-Staged Epoxy Resin," Polymer Engineering & Science, 15(6), pp. 406-414.